Earth and Planetary Science Letters 464 (2017) 211–226

Contents lists available at ScienceDirect

Earth and Planetary Science Letters

www.elsevier.com/locate/epsl

Relationships between lake-level changes and water and salt budgets in the Dead Sea during extreme aridities in the Eastern Mediterranean

Yael Kiro [a,*], Steven L. Goldstein [a,b], Javier Garcia-Veigas [c], Elan Levy [d], Yochanan Kushnir [a], Mordechai Stein [e], Boaz Lazar [f]

[a] Lamont–Doherty Earth Observatory of Columbia University, 61 Route 9W, Palisades, NY 10964, USA
[b] Department of Earth and Environmental Sciences, Columbia University, 61 Route 9W, Palisades, NY 10964, USA
[c] Serveis Cientificotècnics, Universitat de Barcelona, 08028 Barcelona, Spain
[d] Department of Geological and Environmental Sciences, Ben-Gurion University of the Negev, Beer Sheva, Israel
[e] Geological Survey of Israel, 30 Malkhe Israel Street, Jerusalem 95501, Israel
[f] Institute of Earth Sciences, The Hebrew University, Jerusalem, 91904, Israel

ARTICLE INFO

Article history:
Received 28 June 2016
Received in revised form 10 January 2017
Accepted 28 January 2017
Available online 24 February 2017
Editor: M. Frank

Keywords:
lake levels
halite
interglacial
marine isotope stage 5e
Dead Sea
droughts

ABSTRACT

Thick halite intervals recovered by the Dead Sea Deep Drilling Project cores show evidence for severely arid climatic conditions in the eastern Mediterranean during the last three interglacials. In particular, the core interval corresponding to the peak of the last interglacial (Marine Isotope Stage 5e or MIS 5e) contains ∼30 m of salt over 85 m of core length, making this the driest known period in that region during the late Quaternary. This study reconstructs Dead Sea lake levels during the salt deposition intervals, based on water and salt budgets derived from the Dead Sea brine composition and the amount of salt in the core. Modern water and salt budgets indicate that halite precipitates only during declining lake levels, while the amount of dissolved Na^+ and Cl^- accumulates during wetter intervals. Based on the compositions of Dead Sea brines from pore waters and halite fluid inclusions, we estimate that ∼12–16 cm of halite precipitated per meter of lake-level drop. During periods of halite precipitation, the Mg^{2+} concentration increases and the Na^+/Cl^- ratio decreases in the lake. Our calculations indicate major lake-level drops of ∼170 m from lake levels of 320 and 310 m below sea level (mbsl) down to lake levels of ∼490 and ∼480 mbsl, during MIS 5e and the Holocene, respectively. These lake levels are much lower than typical interglacial lake levels of around 400 mbsl. These lake-level drops occurred as a result of major decreases in average fresh water runoff, to ∼40% of the modern value (pre-1964, before major fresh water diversions), reflecting severe droughts during which annual precipitation in Jerusalem was lower than 350 mm/y, compared to ∼600 mm/y today. Nevertheless, even during salt intervals, the changes in halite facies and the occurrence of alternating periods of halite and detritus in the Dead Sea core stratigraphy reflect fluctuations between drier and wetter conditions around our estimated average. The halite intervals include periods that are richer and poorer in halite, indicating (based on the sedimentation rate) that severe dry conditions with water availability as low as ∼20% of the present day, continued for periods of decades to centuries, and fluctuated with wetter conditions that spanned centuries to millennia when water availability was ∼50–100% of the present day. These conclusions have potential implications for the coming decades, as climate models predict greater aridity in the region.

1. Introduction

In many regions of the world droughts are a major concern, affecting agriculture, industry and everyday life. In drought sensitive regions, such as the Middle East, water scarcity impacts political stability. Climate models and observations show a drying trend in the lands around the Mediterranean, reflecting both natural variability and increased anthropogenic greenhouse gas concentrations and predict up to 20% decreases in water availability by the end of the 21st century (Kelley et al., 2012; Lelieveld et al., 2012; Mariotti et al., 2008; Seager et al., 2014). While aridification of the Mediterranean region might be explained by poleward expansion of the Hadley circulation and associated widening of the subtropical dry zone (Frierson et al., 2007), the mechanism and strength of the Mediterranean climate response to increasing greenhouse

* Corresponding author.
E-mail address: ykiro@ldeo.columbia.edu (Y. Kiro).

http://dx.doi.org/10.1016/j.epsl.2017.01.043

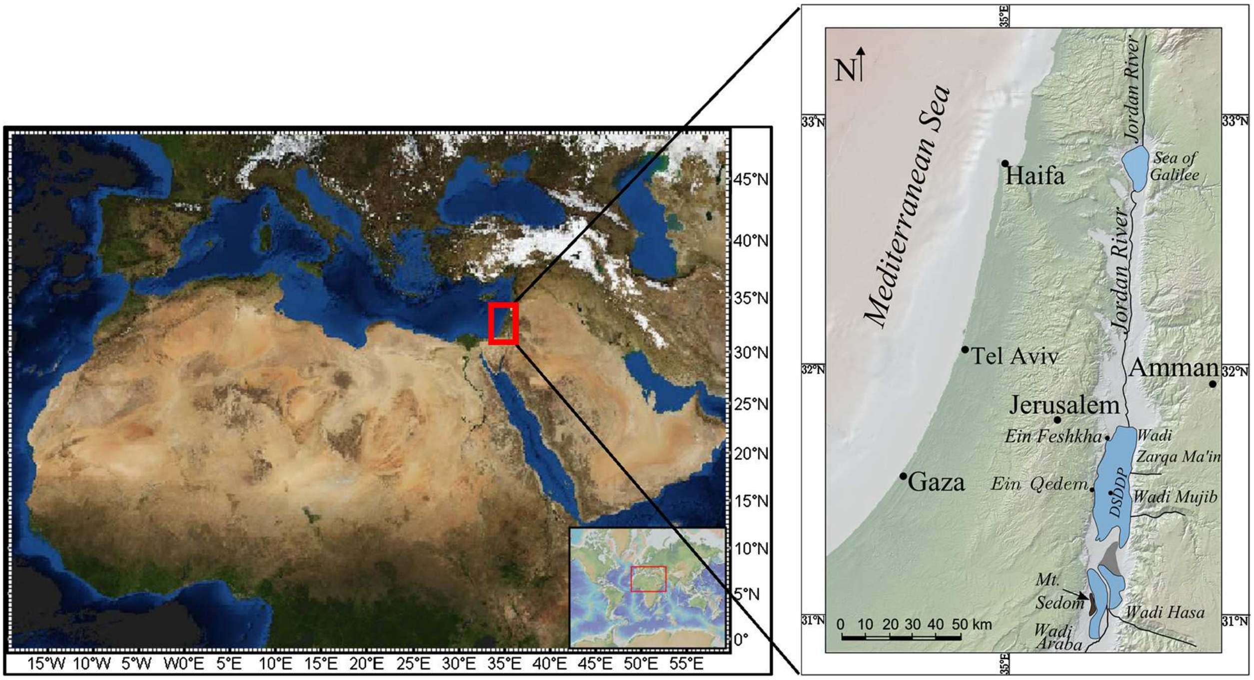

Fig. 1. Location map showing the main water sources into the Dead Sea, and the location of the DSDDP deep core.

gases is not well-understood (e.g. Seager et al., 2014). In the Eastern Mediterranean region, low lake levels in the Dead Sea have been shown to reflect increases in drought frequency that are also associated with higher annual temperatures and northward migrations of storm tracks (Enzel et al., 2003).

The climate during the Holocene and MIS 5e varied both spatially and temporally in the Mediterranean, Europe, North Africa and the Levant (Bar-Matthews, 2014; Damnati, 2000; deMenocal et al., 2000; Harrison et al., 1993; Kushnir and Stein, 2010; Mayewski et al., 2004). The Levant region, comprising Israel, Jordan, Palestine, Lebanon, and Syria, experienced much drier conditions than today, as indicated by halite precipitation in the Dead Sea (Kiro et al., 2016; Neugebauer et al., 2014; Torfstein et al., 2015). Yet, during the last interglacial peak (MIS 5e, ∼130–115 ka), which was characterized by stronger insolation cycles, higher average global temperatures, higher sea levels and smaller continental ice sheets than the Holocene (Dutton and Lambeck, 2012; e.g. Felis et al., 2004; Govin et al., 2015; Kukla et al., 2002; Otto-Bliesner et al., 2013; Rohling et al., 2002), paleoclimate records from the eastern Mediterranean document extended intervals of relatively wet conditions, especially during the peak insolation interval of MIS 5e at around ∼125 ka BP (Bar-Matthews, 2014; Bar-Matthews et al., 2003; Torfstein et al., 2015; Vaks et al., 2007). This wet interval was associated with the tropical northern hemisphere summer insolation peak, which forced intense African summer monsoon rainfall that resulted in increased Nile flow, and the formation of a major sapropel (S5) in the Eastern Mediterranean (Rohling et al., 2002; Rossignol-Strick, 1985; Torfstein et al., 2015; Vaks et al., 2007; Waldmann et al., 2010). Nevertheless, during the past 140 kyr in the Levant, the main source of precipitation moisture has primarily been the Mediterranean Sea (Kolodny et al., 2005; McGarry et al., 2004; Torfstein et al., 2015). Sorting out the hydrological variability in the Levant during the last interglacial and its relation to orbital and global climate variations remains a challenge.

The Dead Sea watershed straddles both the Mediterranean climate zone and the Sahara-Arabian desert belt, reflecting the interplay between these two climate belts. Considering that the effects of anthropogenic warming on the semi-arid and Mediterranean climate is a concern for the future, it is important to know what has occurred in the past, and sedimentary archives provide a means to learn about the severity, duration and frequency of past droughts. The ICDP Dead Sea Deep Drilling Project (DSDDP) recovered such a record from the deep floor of the Dead Sea (Fig. 1) during 2010–2011 (Neugebauer et al., 2014; Stein et al., 2011). The drill site was 297 m below the lake surface, and cores were recovered to a depth of 456 m below the lake floor (mblf), covering ∼200 kyr (Fig. 2 and Torfstein et al., 2015), thus including the Holocene and MIS 5e.

The age model used in this study is constructed mainly after Torfstein et al. (2015), based on U-series dating of aragonite, the lithology of the core, and correlation of aragonite $\delta^{18}O$ in the DSDDP core with $\delta^{18}O$ in the Soreq cave (Bar-Matthews et al., 2003), the marine benthic $\delta^{18}O$ LR04 stack (Lisiecki and Raymo, 2005) and Mediterranean core records (e.g. Wang et al., 2010). For the last glacial maximum to the present-day, the age model is based on the ^{14}C data of Kitagawa et al. (2016). Torfstein et al. (2015) discussed the general paleohydrology of the region, based on the lithology of the core, and showed that the last interglacial was characterized by a high degree of climate variability, with a dry interval marked by halite precipitation during the MIS 6/5 transition, followed by wetter conditions during the peak of MIS 5e without halite precipitation, in turn followed by an extreme dry interval characterized by a thick accumulation of halite.

Here we develop a salt and water budget based on halite fluid inclusions and pore water chemical compositions, together with halite thicknesses from the DSDDP cores. Based on these considerations, we calculate the lake-level changes during the driest intervals in this region and estimate the discharge of water and the amount of precipitation. Our results show that the Levant has experienced severe dry conditions lasting up to a few thousand years during both the Holocene and MIS 5e.

2. Geological and hydrological settings

During the late Quaternary, the Dead Sea basin, the lowest elevation on the continents (the deepest Dead Sea lake floor is >720 mbsl, while the 2016 lake level is at 431 mbsl), was oc-

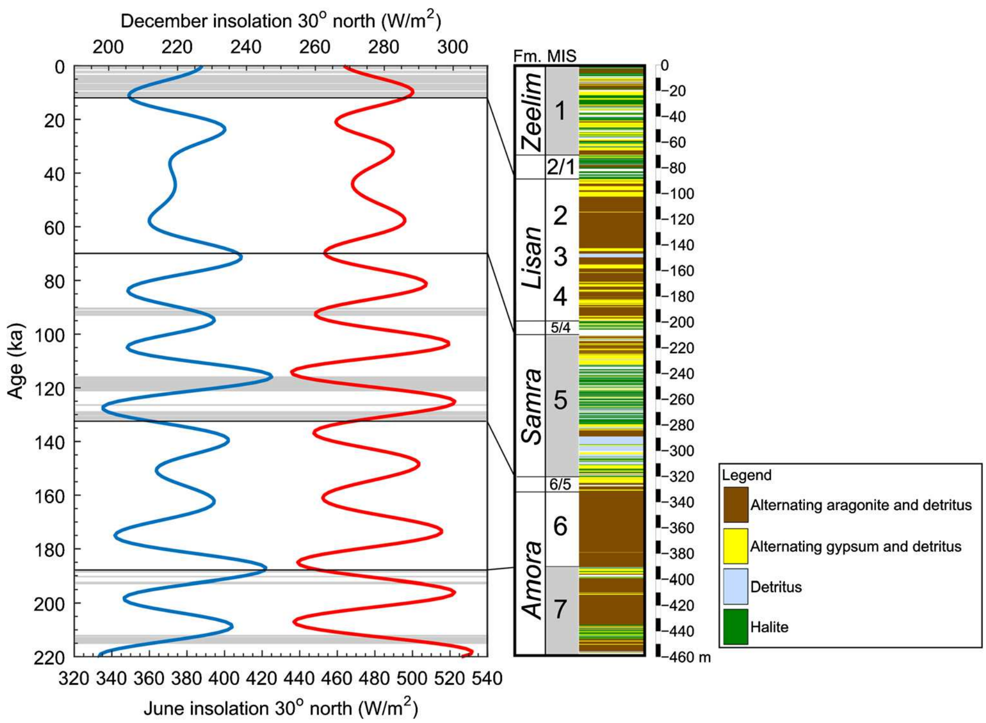

Fig. 2. Stratigraphy of the Dead Sea core. On the left summer (red) and winter (blue) insolation curves for 30° north (Paillard et al., 1996), and the ages of halite layers (in grey). (For interpretation of the references to color in this figure legend, the reader is referred to the web version of this article.)

cupied by a succession of lakes that varied in their compositions and limnological configurations as a result of the changing hydro-climatic conditions in the watershed (Neev and Emery, 1995; Stein, 2001). The modern Dead Sea brine originated from seawater that penetrated the Dead Sea Valley during the late Neogene, forming the Sedom Lagoon (Zak, 1967). The evaporated seawater interacted with Cretaceous limestone surrounding the Valley and produced the Ca-chloride brine that deposited >2000 m of salt in the subsiding Dead Sea basin (Starinsky, 1974; Stein et al., 2000; Zak, 1967). After the Sedom Lagoon became disconnected from the open sea at ∼3 Ma (Matmon et al., 2014; Torfstein et al., 2009), the water-body occupying the Dead Sea Basin became a terminal lake, that was continuously recharged by freshwater from runoff and by saline springs (García-Veigas et al., 2009; Stein et al., 1997; Torfstein et al., 2008) precipitating mainly aragonite, gypsum and halite (e.g. Stein, 2014). The lakes received water, dissolved salts and detritus via runoff from the Jordan and Arava Rivers, smaller rivers, and springs (Fig. 1). The minerals aragonite, gypsum, and halite precipitated, depending on the amount of freshwater inflow and how it mixed with the Dead Sea brine (Katz and Starinsky, 2008; Stein et al., 1997; Torfstein et al., 2008).

Over the late Quaternary, Dead Sea water levels have fluctuated with glacial cycles and have been higher during glacials and lower during interglacials (Bartov et al., 2003, 2002; Stein et al., 2010; Torfstein et al., 2013; Waldmann et al., 2009). For example, over much of the last ice age the lake level fluctuated between ∼300 and ∼250 mbsl, and it rose to ∼170 mbsl during the last glacial maximum high-stand (∼27–24 ka), when it expanded over the present-day Jordan River Valley to north of the Sea of Galilee (Bartov et al., 2002; Hazan et al., 2005; Torfstein et al., 2013). These fluctuations are reflected in the sediment stratigraphy (Fig. 2). The sediments deposited during glacials are mainly primary aragonite and silty-detritus layers of a few mm in thickness that form annual pairs of the *'aad' facies* (Machlus et al., 2000; Prasad et al., 2004) and reflect significant runoff and addition of bicarbonate to the lake. During interglacials, the lake levels are lower, typically at ∼400 mbsl (e.g. the late Pleistocene Lake Samra and the Holocene Dead Sea), and sediments deposited are mostly sequences of silty-detritus (mainly calcite and quartz grains that comprise the *laminated detritus* or *'ld' facies*, Haliva-Cohen et al., 2012). Gypsum-rich sequences were deposited during both interglacials and glacials (Kiro et al., 2016; Migowski et al., 2006, 2004; Neugebauer et al., 2015). They indicate dry intervals associated with abrupt lake-level drops, and reflect $CaSO_4$ saturation following build-up of sulfate in the Ca-chloride brine (Stein et al., 1997; Torfstein et al., 2008, 2005). Halite is deposited only during interglacials and reflects extreme dryness (Fig. 2).

Halite thus indicates high evaporation. It has not been recovered from the marginal terraces, with the exception of an uplifted and tilted late Quaternary halite sequence on the eastern flank of the Mount Sedom salt-diapir (Fig. 1) dated by U–Th to ∼400 ka (possibly MIS 11, Torfstein et al., 2009). With the exception of this halite layer, and modern and Holocene-age deposits along the present-day (human-driven) retreating shore of the Dead Sea, halite deposits over the late Quaternary have been recovered only by drilling. A thick sequence of halite (∼10–20 m) was recovered by drilling to the base of the Holocene on the Dead Sea margin (Migowski et al., 2004; Yechieli et al., 1993), which is dated by ^{14}C at 11–10 ka BP (Stein et al., 2010). Layers of salt have also been recovered by drilling into the Holocene section in the southern basin of the Dead Sea, which was dry during various time intervals (Neev and Emery, 1995).

The present-day Dead Sea is one of the most saline lakes in the world, with a salt content of ∼340 g/L (e.g. Katz and Starinsky, 2008), nearly an order of magnitude higher than seawater. Lake-level fluctuations in the Dead Sea are a function of water discharge into the lake, which is directly related to the regional precipitation (Enzel et al., 2003), because precipitation in the watershed varies more than evaporation from the lake surface (e.g. Lensky et al., 2005; Stanhill, 1994). The volume of evaporating water decreases with declining lake level, due to the decrease in the surface area and lower vapor pressures associated with increases in salinity (Krumgalz et al., 2000; Yechieli et al., 1998), while the volume evaporated increases with

Table 1
The main halite intervals in the Dead Sea core.

Interval depth (m)	Known halite thickness (m)	Estimated halite thickness (m)	Known detritus thickness (m)	Estimated detritus thickness (m)	Age (ka)		Calculated total lake-level drop (m)
390.36–456.7	4.5	8.1	56.1	58.2	188–220	MIS 7	58
328–233.97	29.5	33.4	56.4	60.6	116–134	MIS 5e	239
279.09–233.97[a]	*24.5*	*28.4*	*15.6*	*16.7*	*116–121*	*end of MIS 5e*	*203*
199.21–205.63	3.5	3.7	2.4	2.8	90–93	MIS 5b	26
89.25–0	30.5	33.8	47.9	55.5	0–11.4	MIS 2/1, MIS 1	141

[a] The italics gives the entire thick halite interval of the end of MIS 5e.

increased brine temperature and wind speed (Lensky et al., 2005; Rohling, 2013). The modern Dead Sea evaporation rate, based on energy and mass balances, is 1.05–1.30 m/y (Lensky et al., 2005; Stanhill, 1994; Yechieli et al., 1998), whereas during intervals of greater wetness and lower surface salinity rates may be as high as 1.6 m/y (Stanhill, 1994). During the last glacial period the evaporation rate has been estimated to be considerably higher, between 1.9 and 2.6 m/y (Rohling, 2013). Evaporation rates are expected to decrease in the future due to increasing salinity, for example, down to ~0.7 m/y when the salinity reaches ~460 g/L (Yechieli et al., 1998).

Since the 1960s the freshwater input has decreased significantly due to diversion of the Jordan River and large-scale utilization of freshwater from the Dead Sea watershed. The total amount of freshwater entering the Dead Sea today is only ~300 million m^3/y, compared with ~1600–2000 million m^3/y in the 1950s (Lensky et al., 2005). Together with enhanced evaporation of the brine by potash salt production by Israel and Jordan, the lake level is currently declining at a rate of more than ~1 m/y. In this study, all estimates of water and salt budgets are relative to the natural (i.e., pre-1964) characteristics of the Dead Sea.

3. Methods

Our model is based on the chemical compositions of major elements in the primary fluid inclusions in the halite, and in pore fluids (Levy et al., 2017). Analytical details are in Appendix A, and data are listed in Appendix B. Calculations of brine evolution and halite accumulation rates used the USGS PHREEQC geochemical computer program (Parkurst and Appelo, 2013), using the Pitzer database for calculating ion activity coefficients and water activity in high ionic strength solution according to the Pitzer equations (Pitzer, 1973) in 30 °C. Appendix C lists input and output parameters.

4. Halite distribution in the Dead Sea core

The halite intervals in the DSDDP core occur only during interglacials (MIS 1, 5, 7, Fig. 2, and Table 1), when the lake levels were relatively low (Torfstein et al., 2015). The thickest halite interval occurs during the MIS 6/5 deglaciation and MIS 5e, between ~135 and 116 ka, which contains ~30 m of recovered halite over ~85 m of drilling (~330–235 m depth in the core). Most of the recovered halite (24.5 m over 45 m of drilling at 280–235 m depth in the core) precipitated during the waning stages of MIS 5e between ~122–116 ka. The peak northern hemisphere insolation interval at ~128–122 ka (Fig. 2) is characterized by a ~23 m thick halite-free detritus layer (303–280 m depth in the core), indicating a wetter period (Torfstein et al., 2015). The Holocene halite (89.25–0 m depth in core) is distributed more evenly over time compared with the MIS 5e halite and contains 33.8 m of halite over 89.25 m of drilling.

5. Water and solute budgets

In Section 5.1 we first outline the basis for our conclusion that halite precipitation reflects lake-level drops and negative water budgets in the lake. In Section 5.2 we describe the chemical evolution and precipitation of halite during lake-level drops. Section 5.3 outlines our conceptual model of two stages of halite precipitation, based on the data from the DSDDP core and the changes in the bathymetry of the lake. In Section 5.4 we outline our quantification of the lake-level changes based on the trends of Mg^{2+} and Na^+ in the core, taking into account initial and final concentrations and the thickness of halite. Section 5.5 deals with the fluctuations between wet and dry periods based on the alternating halite and detritus.

5.1. Na, Cl and Mg budgets

The Na^+ and Cl^- budgets in a saline water body are dictated by their removal due to halite precipitation, and contributions from other sources such as fresh water flows and brine discharge. When the Na^+/Cl^- molar ratio in a water body is <1 (the case for Dead Sea brine and for marine and most lacustrine environments), the Na^+/Cl^- ratio decreases during halite precipitation (Fig. 3), and the amount of halite that can precipitate is dictated mainly by the amount of Na. However, dissolution of halite in undersaturated brine adds equal molar amounts of Na and Cl to the brine, increasing the Na^+/Cl^- ratio. At the same time, Mg^{2+} is nearly conservative, as long as Mg-salts are undersaturated, and therefore its concentration decreases during lake-level rise and increases during lake-level drop (Levy et al., 2017). On a long time scale (longer than the 200 kyr represented in the DSDDP core), the Mg^{2+} concentration (hereafter $[Mg^{2+}]$) in the terminal lake should increase due to prolonged input with freshwater (and no precipitation of Mg-salts). However, on the shorter time scales such as the past 200 kyr, lake-level changes have much larger impact on $[Mg^{2+}]$ than the input flux. For example, in the present-day Dead Sea, for a lake-level decline of 20 cm in a year, the amount of Mg^{2+} within the evaporated volume is $\sim 10^{13}$ g, and this amount is added to the residual brine, while the Mg^{2+} flux is nearly two orders of magnitude lower at $\sim 2 \cdot 10^{11}$ g/y (Table 2). Thus, to a first approximation, the $[Mg^{2+}]$ is related directly to lake volume (Fig. 4). We note that $[Mg^{2+}]$ in pore waters reflects the bottom water body during times of a stratified water column. During halite intervals, when the water column of the lake is generally well-mixed, the $[Mg^{2+}]$-volume relationship is direct. During wetter intervals the relationship is affected by water column stratification, and there is probably a delay in the response of $[Mg^{2+}]$ at the bottom of the lake to the volume change.

Here we estimate the water discharge into the Dead Sea, applying salt and water mass balances. Table 2 summarizes the compositions of various water sources in the Dead Sea watershed. Among these sources the potential water sources contributing Na^+ and Cl^- into the modern Dead Sea (prior to the diversion of the Jordan

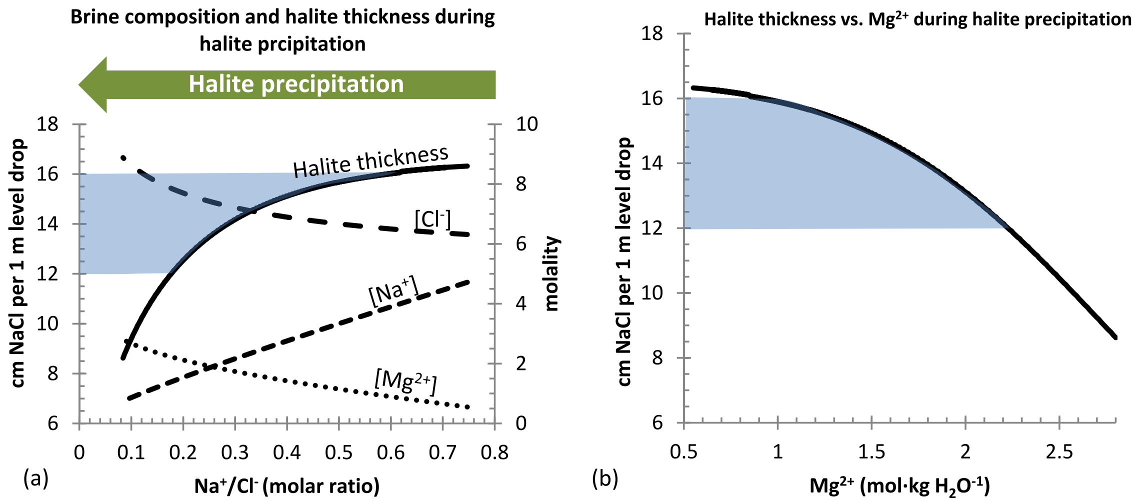

Fig. 3. Changes in chemical compositions and the halite accumulation rate (Eq. (2)) during brine evaporation. (a) vs. Na^+/Cl^+ and (b) $[Mg^{2+}]$. Initial molalities are $[Mg^{2+}] = 0.53$, $[Na^+] = 4.9$ and $[Cl^-] = 6.44$ (more details are in Appendix C). During halite precipitation, in the brine $[Mg^{2+}]$ increases conservatively, the Na^+/Cl^- ratio decreases, and the amount of halite per meter of lake-level drop decreases because of the decrease in $[Na^+]$. The blue field marks the range of compositions of the Dead Sea brines. (For interpretation of the references to color in this figure legend, the reader is referred to the web version of this article.)

Table 2
Water and major element sources into the modern Dead Sea.

	Units	Brine	Jordan River (Arik Bridge)	Jordan River (Dead Sea)	Dissolution of the Sedom formation
Discharge	m^3/y	10^7	$1.2 \cdot 10^9$	$1.2 \cdot 10^9$	
Na^+ concentration	g/m^3	25950	12.2	253	
Cl^- concentration	g/m^3	122500	18.3	474	
Mg^{2+} concentration	g/m^3	20008	9.7	71	
SO_4^{2-} concentration	g/m^3	754	21.3	174.5	
Na^+ flux	g/y	$2.6 \cdot 10^{11}$	$1.5 \cdot 10^{10}$	$3 \cdot 10^{11}$	
Cl^- flux	g/y	$1.2 \cdot 10^{12}$	$2.2 \cdot 10^{10}$	$5.7 \cdot 10^{11}$	
Mg^{2+} flux	g/y	$2 \cdot 10^{11}$	$1.2 \cdot 10^{10}$	$8.6 \cdot 10^{10}$	
SO_4^{2-} flux	g/y	$7.5 \cdot 10^9$	$2.6 \cdot 10^{10}$	$2.1 \cdot 10^{11}$	
Na^+/Cl^- molar ratio		0.32	1	0.83	
Flux in terms of potential accumulation rate of halite	mm/y	0.5	0.03	0.6	~0.2[a]

Data from Bentor (1961); Stein et al. (1997); Salameh and El-Naser (1999); The hydrological service of Israel; Dead Sea surface area is estimated as 600–700 km^2. Potential contribution of the Sedom Formation was calculated according to the rate of uplift (6.2 mm/y, Frumkin, 1996) and multiplied by the diapir area (~14 km^2) divided by the Dead Sea area.
[a] Total halite dissolved during the rise of the diapir was estimated to be 200 m (Zak, 1967). Multiplying this thickness by the Mt. Sedom to Dead Sea area ratio (~14 km^2/~600 km^2, respectively), yields a halite thickness of just ~5 m halite within the Dead Sea.

River during the 1960s) are: brine springs, the Jordan River north of Sea of Galilee and near the Dead Sea, and contributions from Sedom Formation halite.

These values are used to calculate the *potential accumulation rate of halite* on the lake's floor resulting from the annual input flux from these sources (bottom row in Table 2). The mass balance of water and salt translates into halite thickness by the equation:

$$H_R = \frac{\sum_i F_i [\mathrm{Na}]_i \cdot \mu}{\rho \cdot S} \tag{1}$$

where H_R [m/y] is the potential accumulation rate of halite, $[\mathrm{Na}]_i$ [$\mathrm{mol\,L^{-1}}$] is the concentration of Na in a water source i with a flux of F_i [m^3/y], $\mu = 58.433\ \mathrm{g\,mol^{-1}}$ and $\rho = 2170\ \mathrm{g\,L^{-1}}$ are the molecular weight and density of halite, and S [m^2] ($= 600–700 \cdot 10^6\ m^2$) is the Dead Sea surface area. The halite in the Dead Sea core is compacted, with no pores (Kiro et al., 2016), and thus its density is taken as the density of halite. Substituting the values from Table 2 into Eq. (1) yields a potential halite accumulation rate of ~1 mm/y from the pre-1964 input, with brine seepage and the Jordan River as the major Na^+ and Cl^- sources.

The estimated potential halite accumulation rate from the annual input (~1 mm/y) is an order of magnitude lower than the rate of halite deposition of 1–2 cm/y estimated in the DSDDP core (Neugebauer et al., 2014; Torfstein et al., 2015). *Thus, the halite that precipitated in the Dead Sea basin during the last 220 kyr must have originated from evaporation of the brine itself, which in turn means that the halite layers signify declining lake volume.*

However, there is a limit to the amount of halite that can be precipitated by simple evaporation of the Dead Sea brine. For example, a total halite thickness of ~11 m would precipitate by evaporation of the total volume of the modern Dead Sea (Krumgalz et al., 2002). The total amount of halite in the DSDDP core during the last 220 kyr is ~79 m (Table 1). This requires addition of significant salt to the lake. As an example, if we evaporate the water volume of $V \sim 190 \cdot 10^9\ m^3$, corresponding to a lake level of ~350 mbsl when halite starts to precipitate (further discussed below), and if we consider a starting brine composition with a very high potential to precipitate large quantities of halite, such as an $[\mathrm{Na}] = 4.1\ \mathrm{mol\,L^{-1}}$ (Fig. 3) along with a high Na^+/Cl^- ratio, then we would still need at least twice as much Na^+ in order to precipitate the observed 79 m of halite ($T = \frac{[\mathrm{Na}]V\mu}{\rho S} \sim 32$ m where T [m] is the thickness of halite, $\mu = 58.433\ \mathrm{g\,mol^{-1}}$ is the halite molecular weight, $\rho = 2.17 \cdot 10^6\ \mathrm{g\,m^{-3}}$ is the halite density and $S = 650 \cdot 10^6\ m^2$ is the surface area of the lake). Thus, a significant additional supply of Na^+ and Cl^- into the lake is required to precipitate the observed thickness of halite in the DSDDP core.

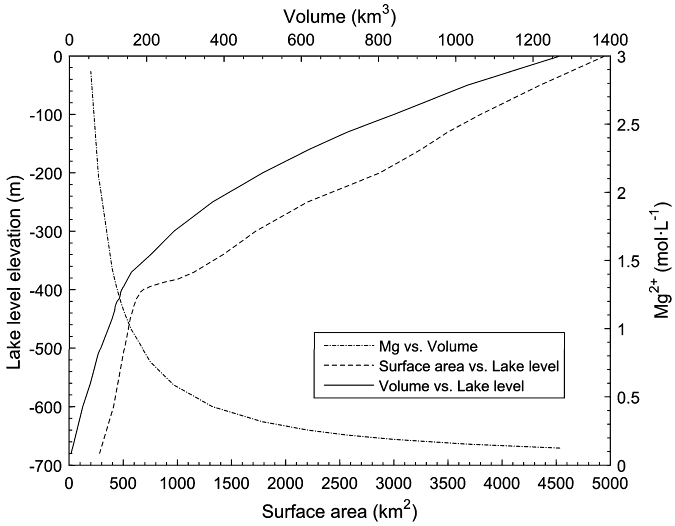

Fig. 4. The Dead Sea hypsometric curve (Hall, 1997) and an example of the variation in [Mg^{2+}] vs. lake volume (discussed in Section 5.3). Due to the topography and bathymetry of the Dead Sea basin, the surface area and volume show significant decreases when lake level decreases from 100 to 400 mbsl, after which the volume and surface area decrease becomes very small. This behavior affects the amount of halite precipitating during lake-level drops (when [Mg^{2+}] increases) as shown in Fig. 3. The [Mg^{2+}] vs. volume plot is calculated according to the relationship between the initial [Mg^{2+}] (0.66 mol L^{-1}) and lake level (320 mbsl) at the onset of halite precipitation during MIS 5e.

The identification and quantification of the additional source is discussed below.

The compositions of Dead Sea brines, as shown in halite fluid inclusions and pore waters, lie on an evaporation curve of the least evolved brine with the least [Mg^{2+}] (Fig. 5). This means that the chemical composition in the brine during the late Quaternary changed mainly due to precipitation and dissolution of evaporite minerals. During the last glacial period (and possibly also MIS 6), dissolution of the Mt. Sedom salt-diapir (Weinberger et al., 2007; Zak, 1967) was a potential source of dissolved salts into the lake (Fig. 1).

The dissolved Na^+ and Cl^- accumulate in the lake when its level and freshwater runoff are high, particularly during glacials, and are removed through halite precipitation when the lake-level drops during interglacials. Thus, during lake-level drops and halite precipitation, any increases in the element concentrations due to fresh water input are negligible compared with decreases due to precipitation of salts as a result of evaporation. For example, Na removal due to a halite precipitation rate of 20 cm/y is $\sim 10^{13}$ g/y, while $\sim 10^{10}$ g/y is added by input from the Jordan River.

5.2. Brine evolution and halite accumulation during evaporation

During lake-level drops and halite precipitation, [Mg^{2+}] increases with the decrease in the lake volume, while [Na^+] and Na^+/Cl^- decrease, and [Cl^-] increases (Fig. 3a). The main constraint on halite precipitation is [Na^+] and therefore the halite accumulation rate decreases as [Na^+] decreases in the brine.

The thickness of halite that accumulates per meter of lake-level drop, assuming a brine saturated with halite, can be calculated according to

$$D = \frac{dH}{dW} \cdot \frac{\mu}{\rho} \tag{2}$$

where D [m-halite/m-lake-level-drop] is the halite accumulation rate, H [mol] is the amount of precipitated halite, and W [L] is the amount of water loss by evaporation, dH/dW is the rate of halite precipitation per amount of water evaporated, $\mu = 58.433$ g mol^{-1} is the molecular weight of halite, and $\rho = 2170$ g L^{-1} is the halite density.

Because the Na^+/Cl^- of the brine varies with salt precipitation and addition (Fig. 5), the Na^+/Cl^- ratio of pore waters and fluid inclusions in halite layers in the core indicates the rate that halite is accumulating (D [m-halite/m-lake-level-drop]) during that time interval (Fig. 3). In the DSDDP core, the range of Na^+/Cl^- ratios is 0.2–0.7 (Fig. 5) indicating that the accumulation rate of halite did not vary much, between $\sim$12 and 16 cm per meter of lake-level drop (Fig. 3).

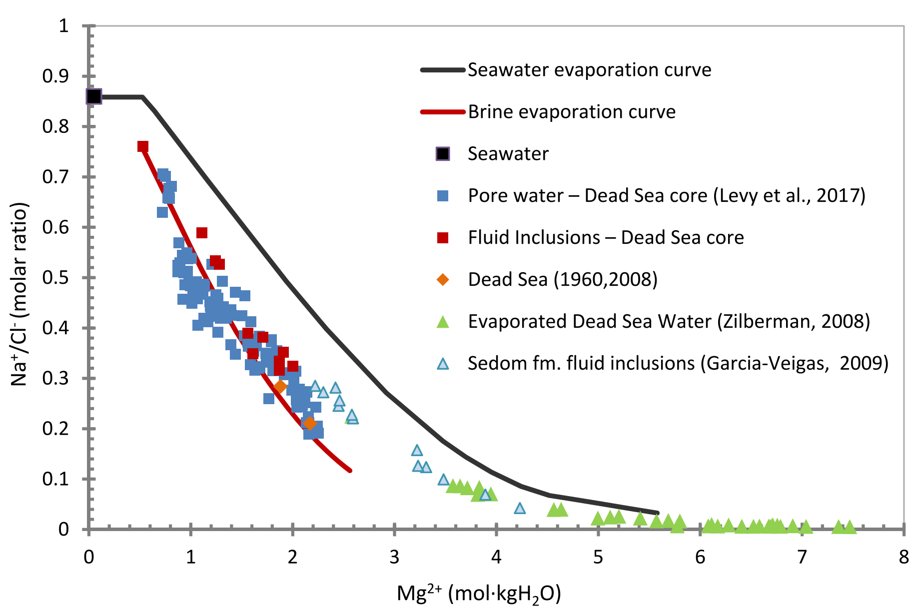

Fig. 5. Na^+/Cl^- molar ratio vs. Mg^{2+} molal concentration in pore waters, halite fluid inclusions and several water bodies (García-Veigas et al., 2009; Zilberman-Kron, 2008) in the Dead Sea basin. The evaporation curves of seawater (black line) and the fluid inclusion with the least [Mg^{2+}] (red line) are shown. The Na^+/Cl^- of the evaporated brine decreases due to halite precipitation while [Mg^{2+}] increases. The DSDDP core pore water and halite fluid inclusions all lie along a single evaporation curve, which is different from seawater. (For interpretation of the references to color in this figure legend, the reader is referred to the web version of this article.)

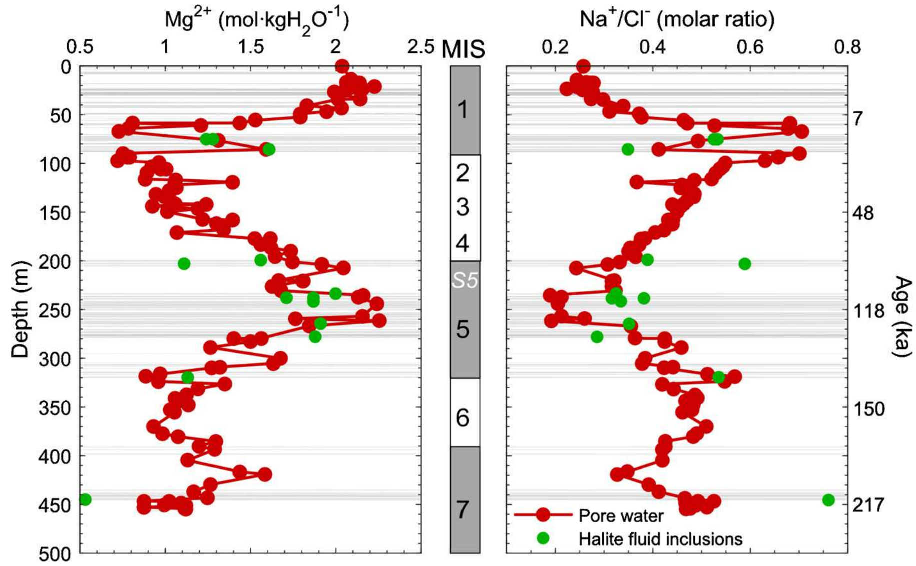

Fig. 6. Mg^{2+} molar concentrations and Na^+/Cl^- molar ratio in pore waters (from Levy et al., 2017) and in halite fluid inclusions (Appendix B) vs depth and age in the DSDDP deep core. Halite layers are marked in grey. During glacials, $[Mg^{2+}]$ decreases and Na^+/Cl^- increases, while during interglacials, when halite precipitates, $[Mg^{2+}]$ increases and Na^+/Cl^- decreases. The core depths here are on a linear scale.

Table 3
Initial and final concentrations of Na^+ and Mg^{2+} during the Holocene and MIS 5e. The second stage of halite precipitation is characterized by slower change in the chemistry and more halite in the lake center.

	Initial Mg^{2+}	Final Mg^{2+}	Initial Na^+	Final Na^+	Change in volume (%)	Halite thickness (m)
	(mol L^{-1})					
Holocene	0.623	1. 667	3.75	1.49	37	41.3[a]
MIS 5e	0.662	1.824	3.09	1.09	36	33.4
Stage 2						
Holocene	1.489	1.667	2.07	1.49	94	16.4
MIS 5e	1.607	1.824	1.71	1.09	88	28.9

[a] Estimated by the thickness of halite in the core during the Holocene (33.8 m) plus estimated marginal halite thickness of 15 m over surface area of 300 km^2 distributed over a lake basin of 600 km^2 (=7.5 m).

5.3. Conceptual model of halite precipitation and lake levels

During halite precipitation, $[Mg^{2+}]$ increases and the Na^+/Cl^- ratio decreases (Fig. 3). Because Mg^{2+} behaves (to a first order) as a conservative ion (that is, its total amount in the lake remains constant), and its concentration is directly related to the lake volume, for any initial lake volume V_i [m^3], the final volume of the lake, V_f [m^3], is described by:

$$V_f = \frac{[\mathrm{Mg}]_i}{[\mathrm{Mg}]_f} \cdot V_i \tag{3}$$

where [Mg] [mol L^{-1}] is the Mg^{2+} concentration and subscripts i and f indicate initial and final, respectively. This relationship between Mg^{2+} and lake volume is directly related to the initial lake surface S_i [m^2] and level L_i [m] via the hypsometric curve of the modern Dead Sea (Fig. 4). According to Eq. (3), the increase in Mg^{2+} from 0.7 to 1.8 mol L^{-1} during MIS 5e, and from 0.6 to 1.7 mol L^{-1} during the Holocene (Fig. 6, the $[Mg^{2+}]$ units in the figure are in molality) is equivalent to lake volume decreases to ~40% during both time periods (Table 3). Fig. 4 shows that the increase of the Mg^{2+} during MIS 5e corresponds to a lake-level change from ~320 to 490 mbsl (where the initial $[Mg^{2+}]$ and lake level are those at the beginning of MIS 5e).

Comparison of the amount of halite precipitated with $[Mg^{2+}]$ in the DSDDP core reveals that there are two stages (illustrated by the MIS 5e data, Fig. 7). During Stage 1 there is a large increase in Mg^{2+} with little halite (from 0.7 to 1.6 mol L^{-1} over a 4.5 m thick halite layer), while during Stage 2, a lot of halite precipitates with

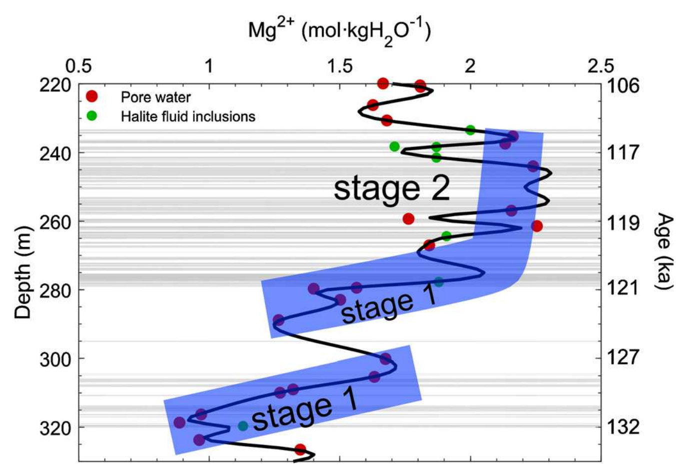

Fig. 7. Mg^{2+} molal concentrations in pore waters and halite fluid inclusions in the MIS 5e interval. Halite layers are grey lines. The bands mark the general trend of $[Mg^{2+}]$ during precipitation of halite and the two stages (Section 5.3). During Stage 1 $[Mg^{2+}]$ increases sharply while a small thickness of halite accumulates, while during Stage 2 $[Mg^{2+}]$ increases a small amount while a large thickness of halite accumulates. The smaller increase of $[Mg^{2+}]$ during Stage 2 is probably due to halite dissolution at the lake's margins and its re-precipitation in the deep basin (halite focusing, shown in Fig. 8).

little increase in Mg^{2+} (from 1.6 to 1.8 mol L^{-1} over a 28.9 m thick halite layer). In stark contrast to the 28.9 m of halite observed during Stage 2, the calculated thickness of halite expected from the changes in Mg^{2+} and Na^+ is only ~4 m. This indicates that the

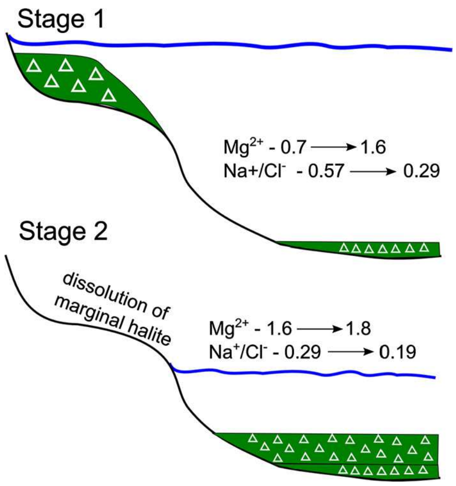

Fig. 8. Conceptual model describing halite precipitation and halite focusing during MIS 5e lake-level drop. Stage 1: At lake levels higher than ∼400 mbsl, halite precipitates both at the margins and in the middle of the lake. Stage 2: Halite focusing. Due to the basin topography, at low lake levels the marginal halite dissolves and re-precipitates at the center of the lake. The increase in $[Mg^{2+}]$ per cm of salt precipitated is much higher during Stage 1 than during Stage 2 (Fig. 7). Dissolution of marginal halite by fresh water decreases $[Mg^{2+}]$ and increases the Na^+/Cl^- ratio, leading to the deposition of thick layers of halite with small changes in the Mg^{2+}.

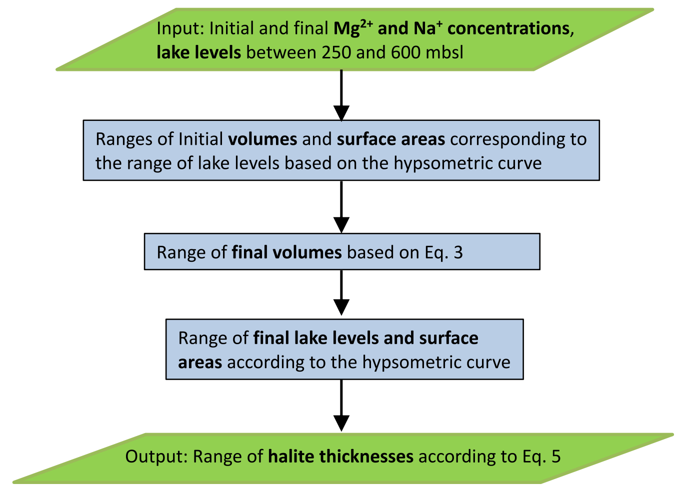

Fig. 9. A flow chart of the model used to calculate halite thicknesses as a function of lake levels and changes in $[Na^+]$ and $[Mg^{2+}]$.

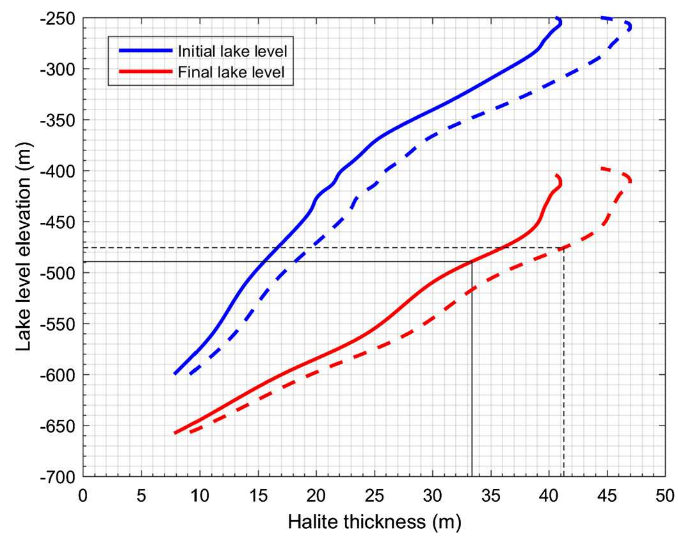

Fig. 10. Initial (blue) and final (red) lake levels vs halite thickness, based on changes in $[Mg^{2+}]$ and $[Na^+]$ (Section 5.4, Table 3) during MIS 5e (solid) and the Holocene (dashed). The estimated halite thicknesses during the Holocene and MIS 5e are ∼41 and ∼33 m, respectively, corresponding to initial and final lake levels of 308 and 475 mbsl during the Holocene and 320 and 490 mbsl during MIS 5e, respectively. (For interpretation of the references to color in this figure legend, the reader is referred to the web version of this article.)

decreases in lake volume were not the sole factor determining the amount of halite that precipitated in the middle of the lake (details are in Section 5.4, and relationships between halite precipitation, Na^+ and Mg^{2+} are described by Eqs. (4), (5)).

The two stages of halite precipitation (Fig. 7) are related directly to the lake's hypsometric curve (Fig. 4), which shows an inflection point at ∼400 mbsl, reflecting important changes in the geometry of the basin, whereby the slope of the margins is much steeper below that elevation. As a result, at lake levels higher than 400 mbsl, for each meter of lake-level change there are much larger changes in volume and surface area, than at lake levels below 400 mbsl.

The basin geometry has important impacts on halite deposition at the lake margins versus the middle (Fig. 8). During Stage 1, when lake levels are above 400 mbsl, thicker layers of halite are deposited at the lake margins than in the center. For example, along the margins of the Holocene Dead Sea there is a ∼15 m thick halite layer that precipitated between ∼10.7 and 10.2 ka (Stein et al., 2010), while only ∼7.7 m are found in the deep DSDDP core. However, halite is generally absent in the marginal sections of the Dead Sea, because the marginal salt is re-dissolved and added back to the lake brine, to be re-precipitated in the lake center. As a result, for each meter of lake-level drop during Stage 2 there is more halite precipitated in the center of the basin. Therefore, the halite recovered from the DSDDP core, at the depocenter of the lake, comprises most of the halite that deposited in the entire basin. These relationships, that is, the changes in chemical composition and the total thickness of halite, can be used to calculate changes in lake levels. In Section 5.4 below we outline our method to quantify lake-level changes based on the initial and final concentrations of Mg^{2+} and Na^+ assuming that all the halite is re-precipitated in the lake center.

5.4. Reconstructing lake-level changes and average fresh water runoff

The lake-level changes are calculated using the halite thicknesses, the Mg^{2+} and Na^+ concentrations in the lake brine (Table 3), and the lake's hypsometric curve (Fig. 4), through a halite interval in the DSDDP core, such as MIS 5e or the Holocene (Table 1). The use of the hypsometric curve yields a single solution for initial and final lake levels for each of the halite intervals (Figs. 9, 10).

The model calculates the initial and final lake levels as described in a flow chart (Fig. 9). Given an initial volume V_i [m^3], the final lake surface area S_f [m^2], lake level L_f [m], and volume V_f [m^3] are all related by Eq. (3) and the Dead Sea hypsometric curve. The amount of halite H [mol] that is precipitated can be calculated from the change in $[Na^+]$ (Table 3) by

$$H = \left([\mathrm{Na}]_i \frac{[\mathrm{Mg}]_f}{[\mathrm{Mg}]_i} - [\mathrm{Na}]_f\right) V_f \tag{4}$$

where [Na] [mol m^{-3}] is the Na^+ concentration. Assuming an evenly distributed halite layer precipitates over the final lake surface (Section 5.3), the thickness of halite T [m] is a function of the surface area, and can be calculated by:

$$T = \frac{H}{\rho \cdot S_f} \cdot \mu = \frac{([\mathrm{Na}]_i \frac{[\mathrm{Mg}]_f}{[\mathrm{Mg}]_i} - [\mathrm{Na}]_f) V_f}{\rho \cdot S_f} \cdot \mu \tag{5}$$

for any given initial volume V_i [m^3], where V_f [m^3] is calculated by Eq. (3). S_f [m^2] is the final surface area correspond-

Table 4
Modeled initial and final lake levels, discharge to the lake, and rainfall during the Holocene and MIS 5e.

	Initial lake level (m)	Final lake level (m)	Average discharge (million m^3/y)	% of modern discharge	Average precipitation in Jerusalem (mm/y)	% of average modern precipitation
Holocene	−308	−475	580–690	30–50	300–400	50–67
MIS 5e	−320	−490	560–670	30–50	300–400	50–67

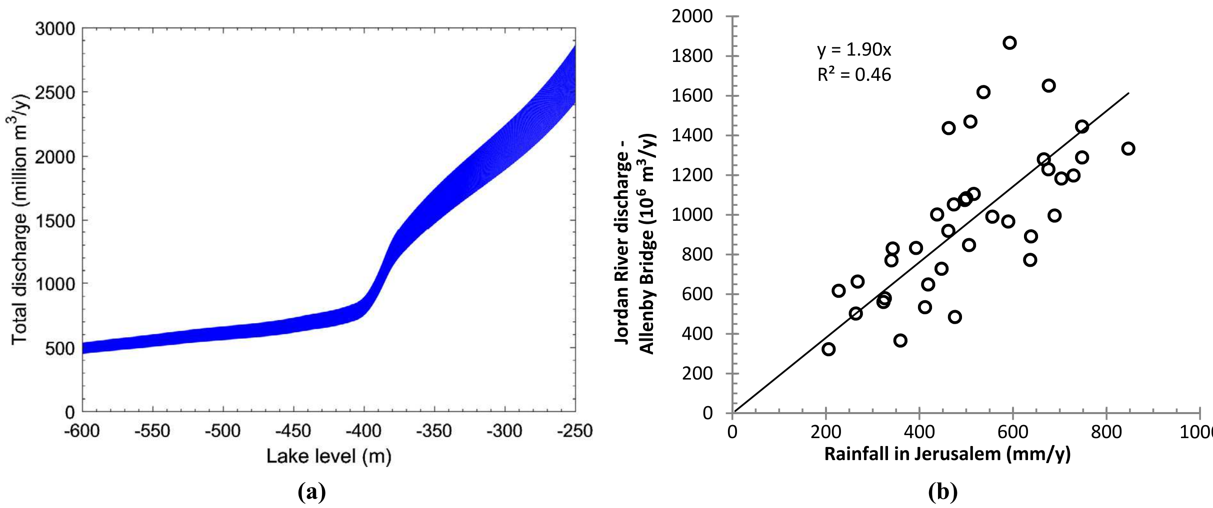

Fig. 11. Relationships between lake levels or rainfall in Jerusalem and runoff to the Dead Sea. (a) The calculated total discharge to the Dead Sea vs lake level (based on an evaporation rate of 1.1–1.3 m/y; Lensky et al., 2005; Stanhill, 1994) and a surface area based on the Dead Sea hypsometric curve (Hall, 1997). (b) Jordan River discharge (∼70% of total discharge) vs rainfall in Jerusalem between 1928 and 1965 (data is from the Israel Meteorological Service and the Israel Water Authority).

ing to V_f according to the hypsometric curve (Fig. 4), and $\mu = 58.433\ \mathrm{g\,mol^{-1}}$ and $\rho = 2.17 \cdot 10^6\ \mathrm{g\,m^{-3}}$ are the molecular weight and density of halite, respectively. Uncertainties regarding these assumptions are discussed in Appendix D. Thus *the thickness of halite deposited can be calculated for any given initial lake-level elevation* (Figs. 9, 10).

Lake levels versus halite thickness calculated for the Holocene and MIS 5e periods are plotted in Fig. 10, which shows this relationship for a *range* of initial lake-level elevations. The calculation indicates that in order to precipitate the amount of halite observed in the DSDDP core, the lake level dropped by ∼170 m during both the Holocene and MIS 5e, from 308 mbsl and 320 mbsl at the end of the MIS 2 and MIS 6 glacials, to lake levels of 475 and 490 mbsl, respectively (Table 4). We note that the thickness of Holocene halite takes into account 7.5 m of non-dissolved marginal halite (Section 5.3 and Table 3), while this is not the case for the MIS 5e estimate because there is no evidence for non-dissolved marginal halite from that time in the DSDDP cores from the near-shore sites (Neugebauer et al., 2015).

In order to reach these low lake levels, the average water discharge into the lake would have to be very low. Plotting the discharge to the lake as a function of the lake-level (Fig. 11a) as calculated from the evaporation rate of 1.1–1.3 m/y (Lensky et al., 2005; Stanhill, 1994) and the hypsometric curve (Fig. 4) indicates that during the interglacials, the annual discharge was just ∼40% of the modern (pre-1964) value.

The modern multi-year averaged precipitation over the Dead Sea watershed region has been correlated with the instrumental rainfall record in Jerusalem for the years 1870–1960, and with other stations in the Levant region (Enzel et al., 2003). This is the longest existing southern Levant rainfall record. Using the modern Jerusalem rainfall record, a discharge of 40% of the modern (pre-1964) value into the Dead Sea (∼$600 \cdot 10^6\ \mathrm{m^3/y}$) during the Holocene and MIS 5e salt intervals implies that the average rainfall in Jerusalem decreased to ∼350 mm/y, which is ∼60% of the modern average rainfall of 605 ± 195 mm/y (average and standard deviation of precipitation in Jerusalem between 1865–1995; Israel Meteorological Service, Table 4, Fig. 11b). On decadal time scales, the Jerusalem record varies in concert with less continuous precipitation records from Beirut and Damascus in the north to Beer Sheva in the south (Enzel et al., 2003; Kushnir and Stein, 2010). Therefore we assume that the changes in Jerusalem are representative of the whole region. Uncertainties of these estimates are discussed in Appendix D.

The Levant region sporadically experiences years with low precipitation and droughts, and the annual rainfall varies significantly from year to year. According to the instrumental rain record, clusters of years with only ∼300 mm/y in Jerusalem occur occasionally and are considered very dry intervals. According to modern observations, between 1864 and 1995 rainfall lower than 400 mm/y occurred on average every 8 years. Two nearly decade-long, historical dry intervals centered on 1930 and 1960 (Kushnir and Stein, 2010). Based on the modern instrumental data, lake-level declines were correlated to time intervals when 50% of the years experienced less than 450 mm/y (Enzel et al., 2003). Based on the modern data, Enzel et al. (2003) concluded that low lake levels during the past 4000 years reflect long periods when the annual rainfall fell frequently below the modern average. Using the modern comparison between lake levels and regional annual precipitation to infer the past, our results thus indicate that during the interglacial salt intervals, average precipitation was extremely low, with high frequency of years with severe droughts during which annual precipitation was much lower than 350 mm/y.

5.5. Fluctuations between wetter and drier intervals

Despite the overall extremely arid conditions that prevailed in the Eastern Mediterranean during MIS 5e and early Holocene, the salt intervals in the DSDDP core show alternations between layers of halite and detritus (Fig. 2) indicating fluctuations between drier and wetter intervals. This means that the dry intervals were punctuated with periods of wetness and increasing lake levels even though overall the lake level was declining. Within the core, different halite facies also reflect changes between dryer and wetter conditions, often showing seasonal changes represented by different types of crystals (Kiro et al., 2016). The halite layers contain two main crystal types, large crystals that precipitate at the lake bottom, and small cumulate crystals that precipitate at the lake surface. The large crystals reflect wetter conditions than the small cumulate crystals, and they are associated with more detritus and show effects of mild dissolution (Kiro et al., 2016). Frequent alternations between these two crystal types are seasonal, with the large "bottom-growth" crystals forming during winter and the small cumulates during summer (Kiro et al., 2016). The seasonal halite layers range in thickness between ~0.5–2 cm implying sedimentation rates between ~1–4 cm/y, while a typical sedimentation rate is ~2 cm/y.

The average lake-level drop during the whole MIS 5e halite interval (between 328 and 234 m in the DSDDP core) is ~1 cm/y, taking into account detritus-rich layers. However, during halite rich intervals rate of lake-level drop was much higher. Based on estimates of the halite sedimentation rates, and 12–16 cm of halite precipitated per meter of lake-level drop (Fig. 3), we conclude that the lake-level drop rate during halite-rich intervals was between 6 and 33 cm/y ($L_r = S_r/D$ where L_r [cm/y] is the lake-level drop rate, S_r [m/y] is the sedimentation rate and D [cm/m] is the thickness of halite precipitated per meter lake-level drop). Based on this rate of lake-level drop, an evaporation rate of 1.1 m/y, and a surface area of 560 km^2, corresponding to a lake level of 450 mbsl (Fig. 4), we calculate that the most arid intervals, reflected by the thick cumulate layers of halite, are characterized by an annual discharge of only ~430 million m^3/y ($(1.1–0.33) \cdot 560 \times 10^6$), which is ~20% of the modern (pre-1964) value. A caveat to this calculation is that the distribution of halite might not be homogeneous beneath the lake surface. As discussed in Section 5.3, at least during the Stage 1 of halite precipitation (reflected by rapid changes in [Mg^{2+}] in the Dead Sea brine, Fig. 7), the halite layers are thicker on the lake margins compared with the center. In this case, the estimated discharge would be even lower.

The halite thicknesses indicate that the most arid intervals lasted for decades to centuries: in between >1 m intervals of halite-free detritus, the average thickness of halite layers is $\sim 1.7 \pm 1.4$ m (1SD). These extreme arid conditions fluctuated with milder conditions, as reflected by the detritus intervals that indicate increases in the lake level lasting up to a few thousand years. During the peak of MIS 5e, a 23 m thick detritus layer indicates a wet period that lasted several thousands of years (~128–122 ka, at ~303–280 m depth in the DSDDP core, Torfstein et al., 2015). This was coeval with a major sapropel event in the Eastern Mediterranean (the 'S5' event; e.g. Cane et al., 2002; Rohling et al., 2002; Rossignol-Strick, 1985), when deep water in the Mediterranean became anoxic as a result of a major increase in the Nile flux. During this period in the Dead Sea, [Mg^{2+}] decreased from ~1.68 to $\sim 1.27\ \mathrm{mol\,kg\,H_2O^{-1}}$ (Fig. 6). This indicates that the lake level increased from ~470 mbsl to at least 411 mbsl (Figs. 4, 7; the lake level at the end of Stage 1 of halite precipitation is calculated according to Eq. (5)) due to increased discharge (to >760 million m^3/y, >50% of modern), as estimated from the lake-level rise or surface area and evaporation rate (Fig. 11a).

In summary, the characteristics of the halite-rich and detritus-rich intervals during the interglacials can be used to estimate the water discharge and duration of these cycles. Given the detritus and halite deposition rates and thicknesses, together with the calculated discharge to the lake, it follows that the climate fluctuated between extremely arid periods (with water availability ~20% of present day) spanning decades to centuries (15–300 y), and wetter periods (water availability 50–100% of present day) spanning centuries to millennia (90–6000 y).

6. Levant climatic context

Our knowledge of the Levant regional climate during MIS 5e (Bar-Matthews, 2014; Develle et al., 2011; Lazar and Stein, 2011; Petit-Maire et al., 2010; Torfstein et al., 2015; Vaks et al., 2006; Waldmann et al., 2010) is not extensive, and tends to emphasize high precipitation (Bar-Matthews, 2014). For example, δ^{18}O and δ^{13}C in speleothem records (e.g. Soreq cave, Bar-Matthews, 2014), have been interpreted as indicating higher amounts of precipitation in the region compared to present-day (Bar-Matthews et al., 2003). Torfstein et al. (2015) highlighted the climatic variability during this time interval based on the DSDDP core record, which indicates lake-level decline during the MIS 6/5 deglaciation between ~135–128 ka, a wet period during the MIS 5e peak insolation interval between ~128–122 ka as indicated by mud layers and an absence of halite, followed by extreme aridity to ~115 ka. The wetter interval in the core coincides with the ages of the speleothems (Vaks et al., 2006) and travertine deposition (Waldmann et al., 2010) in the southern Negev desert as well as ages of diagenesis by freshwater of coral reefs in the more generally hyperarid Gulf of Aqaba (Lazar and Stein, 2011; Yehudai et al., 2017). Our record and our lake-level estimates however, clearly show that the whole MIS 5e interval was *on average* much drier than today.

As an alternative to high amounts of precipitation in the region between 128–122 ka, moisture originating in a tropical source (Torfstein et al., 2015; Vaks et al., 2006), or an increase in rainfall intensity per event, could also explain the increased wetness indicated by the DSDDP record and the δ^{18}O in Soreq cave speleothems. In this case, the increased precipitation could reflect changes in the temporal and spatial distribution of rainfall, and fluctuations between relatively wetter conditions similar to the present-day and more extreme arid conditions.

During MIS 5e the summer insolation peak was higher than during the Holocene (Berger and Loutre, 1991). Moreover, the difference between summer and winter insolation was greater, indicating greater seasonal contrast. This is seen in temperature proxies (δ^{18}O, Sr/Ca) of Red Sea corals, which show increased seasonal contrast at the peak of the last interglacial (Felis et al., 2004). Moreover, according to climate models, winters during this time interval (characterized by very low insolation in the northern hemisphere) were warmer over Europe and colder over the south and central Levant compared to pre-industrial climate (Felis et al., 2004; Otto-Bliesner et al., 2013). The colder winters in the Levant and warmer winters over Europe have been associated with wetter winters in the southern Levant (Felis and Rimbu, 2010; Kushnir and Stein, 2010).

While there has been significant Holocene climate variability in the Levant, it was not as variable in time and space as during MIS 5e. For example, Holocene δ^{18}O and δ^{13}C in speleothem records from Soreq cave do not vary as much as during MIS 5e (Bar-Matthews et al., 2003), and there is no evidence of increased precipitation at the edges of the desert belt, as represented by the MIS 5e speleothems in the Negev (Vaks et al., 2006). Nevertheless, the presence of Holocene salt in the DSDDP core, and our reconstructed water-budget, as well as significant hiatuses in the sedimentary records of the marginal terraces of the Dead Sea (Migowski et al., 2006) indicate that the early Holocene period was on average drier than today. Both lake levels (Migowski et al., 2006) and the DSDDP core halite sequences (Fig. 12) show that the climate varied between conditions slightly wetter than today and extremely dry (when lake level was low and halite precipitated).

Several studies have discussed changes in spatial pattern of the climate variability in the Levant and Middle East on interannual to multidecadal time-scales, and refer in particular to variations in precipitation (Cook et al., 2016; Cullen and deMenocal, 2000;

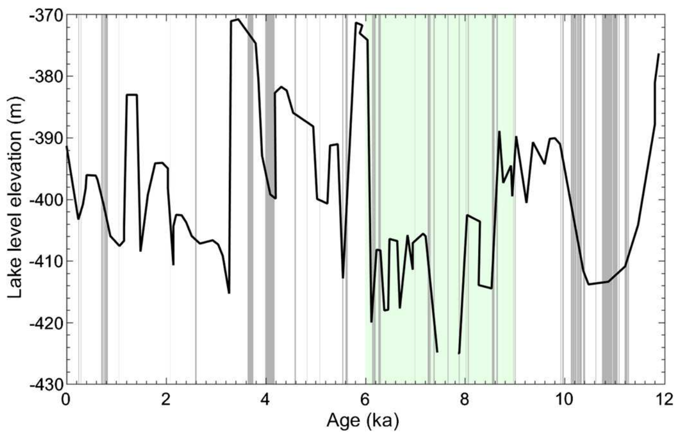

Fig. 12. Halite layers (in grey) and lake levels during the Holocene. The lake-level curve is from Kushnir and Stein (2010) and Stein et al. (2010), and uses their ages. The halite layers are from the DSDDP stratigraphy, the DSDDP age model for this interval is derived from Kitagawa et al. (2016). There may be some small discrepancies between low lake levels and halite layers due to inconsistencies in the age models. The green area marks the peak of the African Humid Period (deMenocal et al., 2000). (For interpretation of the references to color in this figure legend, the reader is referred to the web version of this article.)

Feliks et al., 2010; Felis et al., 2000; Felis and Rimbu, 2010; Kushnir and Stein, 2010). The major pattern of precipitation variability in the modern record is associated with the North Atlantic Oscillation/Arctic Oscillation (NAO/AO), the two paradigms of a prominent mode of Northern Hemisphere, low-frequency circulation variability (Hurrell et al., 2001; Wallace, 2000). The NAO/AO is particularly strong in winter (December–March) when it represents changes in the intensity and position of the permanent pressure centers in the North Atlantic, together with meridional swings in the Atlantic jet stream and storm tracks that significantly impact the Mediterranean Basin. A positive phase of the NAO, with a deep Icelandic Low and strong Azores High, is associated with a colder and wetter than normal climate in the Levant (Givati and Rosenfeld, 2013; Kushnir and Stein, 2010) and the southeastern Mediterranean (Egypt and Libya; Felis and Rimbu, 2010; Givati and Rosenfeld, 2013), while in the countries of the Mediterranean northern rim, over Turkey and south Europe, the climate is drier than normal (Cullen and deMenocal, 2000; Felis and Rimbu, 2010). The DSDDP cores record the southern Levant climate.

Comparison of the Levant climate to higher and lower latitudes can be used to infer the changes in the meridional variability during the Holocene and MIS 5e. More paleoclimatic records, and with higher resolution, are available during the Holocene compared with MIS 5e. During MIS 5e, pollen records from Europe indicate a warm and wet climate (e.g. Brauer et al., 2007; Kukla et al., 2002). The southern Sahara desert (Osborne et al., 2008; Smith et al., 2007; Szabo et al., 1995) and Arabia (Rosenberg et al., 2013) climate records also show wetter episodes particularly during the peak summer insolation interval of MIS 5e, when the increase in precipitation is associated with the intensification of the African summer monsoon and the northward contraction of the desert boundary (Battisti et al., 2014; Herold and Lohmann, 2009). However, while the wet episodes in the desert belt during MIS 5e coincide with the relatively wetter interval in the Levant and temporary rises in lake levels, it was not so during the Holocene African Humid Period (deMenocal et al., 2000), when the Dead Sea lake levels were low and halite precipitated (Fig. 12). At that time, most of Europe was relatively wet, but lakes in southern Europe were in phase with the Dead Sea levels (Harrison et al., 1993). The higher summer insolation peak and the greater difference between summer and winter insolation during MIS 5e compared to the Holocene (Berger and Loutre, 1991) may explain the different response of Levant climate in these two time intervals.

7. Summary

This study uses brine compositions measured in fluid inclusions in salts and pore waters, and the thicknesses of salt layers (recovered from coring of the deepest basin of the Dead Sea by the ICDP Dead Sea Deep Drilling Program) to calculate water and salt budgets during the last interglacial MIS 5e and the Holocene, and infer the hydro-climatic conditions.

The calculations show that the climate was significantly drier than the present-day during MIS 5e and much of the Holocene. Lake levels decreased from ∼308 and ∼320 mbsl to ∼475 and ∼490 mbsl during the early Holocene and MIS 5e, respectively, resulting in substantial halite deposition, with 33.4 and 33.8 m during MIS 5e and the Holocene, respectively. The lake level decreases were associated with significant reductions in average fresh water inputs to the lake, to ∼30% of the present-day discharge in both the Holocene and MIS 5e and lasting over thousands of years. Nevertheless, during these major dry intervals, halite deposition alternated with halite-free detritus deposition, indicating a persistent pattern of intermittent flooding events when the discharge was >50% of the modern amount. These water discharge estimates and lake levels indicate that during the interglacial salt intervals the average precipitation in the Eastern Mediterranean was extremely low, with high frequency of years experiencing severe droughts, and with precipitation in Jerusalem <350 mm/y, compared to ∼600 mm/y today. We use the halite and detritus sedimentation rates and the calculated lake-level changes to estimate the water discharge and duration in cycles within the interglacials. The halite-rich-detritus-rich cycles reflect fluctuations between extreme dry periods, with water availability as low as 20% of the present day spanning decades to centuries (15–300 y), and wetter periods with water availability of ∼50–100% of the present day spanning centuries to several millennia (90–6000 y).

The DSDDP salt record documents intervals during the last interglacial and the early Holocene characterized by much more severely arid conditions than those predicted by global climate models (e.g. the forecast of a ∼20% decrease in water availability around the Mediterranean due to warming by the end of the 21st century, Mariotti et al., 2008). Because what happened in the past may happen again, this study's findings may have implications for future water resources in the densely populated East Mediterranean–Levant.

Acknowledgements

We thank Ittai Gavrieli, Yehouda Enzel, Efrat Morin, Abraham Starinsky and Amitai Katz for their insights and helpful comments. We are very grateful to the reviewers, whose comments helped to improve the paper significantly. This study was supported by the US–Israel Bi-National Science Foundation (USIBSF, grant #2010375 to SLG and MS), the Dead Sea Drill Excellence Center of the Israel Science Foundation (grant #1736/11 to BL), the Storke Endowment of the Department of Earth and Environmental Sciences of Columbia University and the US NSF (grant # EAR-1635391 to YK, SLG and YK). This is Dead Sea Excellence Center contribution #13 and LDEO contribution #8089.

Appendix A. Methods

The chemical compositions of major elements in primary fluid inclusions within the halite were measured using cryo-SEM-EDS (cryo unit: ALTO 1000, GATAN; SEM: J-6510, JEOL; EDS Inca, OXFORD INSTRUMENTS) at the Universitat de Barcelona following the method of Garcıa-Veigas (1993), Ayora et al. (1994) and

Table B1

Sample	Depth	Na	s.d.	Mg	s.d.	Cl	s.d.	K	s.d.	Ca	s.d.	Na/Cl	Mg/Ca
ky119	75.40	3.56	0.07	1.24	0.05	6.68	0.04	0.19	0.02	0.23	0.05	0.533	5.4
ky118	75.47	3.53	0.08	1.28	0.06	6.71	0.09	0.15	0.03	0.22	0.02	0.526	5.8
ky132	85.41	2.42	0.14	1.61	0.07	6.93	0.06	0.21	0.01	0.52	0.02	0.349	3.1
ky88	199.15	2.69	0.04	1.56	0.02	6.91	0.07	0.18	0.02	0.45	0.01	0.389	3.5
ky93	202.90	3.98	0.09	1.11	0.02	6.76	0.08	0.11	0.01	0.2	0.02	0.589	5.6
ky6(4)	233.48	2.36	0.05	2.00	0.32	7.28	0.52	0.18	0.07	0.34	0.12	0.324	5.9
ky13(18)	238.25	2.68	0.03	1.71	0.09	7.02	0.14	0.17	0.04	0.35	0.05	0.382	4.9
ky13(13)	238.30	2.31	0.10	1.87	0.28	7.31	0.39	0.25	0.07	0.5	0.01	0.316	3.7
ky74	241.40	2.40	0.05	1.87	0.07	7.19	0.04	0.19	0.02	0.37	0.01	0.334	5.1
ky42(7)	264.33	2.47	0.11	1.91	0.14	7.02	0.07	0.17	0.03	0.31	0.04	0.352	6.2
ky71c	277.78	2.00	0.06	1.88	0.02	7.01	0.07	0.14	0.01	0.51	0.02	0.285	3.7
ky76	319.70	3.66	0.05	1.13	0.03	6.84	0.05	0.23	0.02	0.35	0.03	0.535	3.2
ky80	445.23	4.90	0.07	0.53	0.03	6.44	0.03	0.13	0.02	0.16	0.01	0.761	3.3

Lowenstein et al. (2016). Fluid inclusion sizes varied between 5 and 40 μm. Quantitative analyses were based on linear regressions of the X-ray peak-to-background ratio of each component in the EDS spectra of single fluid inclusions and of four standard solutions with a similar matrix. The detection limits of this method in mol kg H_2O^{-1} are 0.20 (Na), 0.05 (Mg and S), 0.01 (Ca and K). Final concentrations calculated assume solutions that are charge balanced and saturated with halite.

Appendix B

Element concentrations (mol kg H_2O^{-1}) in halite fluid inclusions measured by cryo-SEM. Errors are in 1 standard deviation (1 s.d.) over concentrations in 5–10 fluid inclusions, see Table B1.

Appendix C. Input and output parameters for halite accumulation calculation during lake-level drop using PHREEQC

The initial brine composition was chosen to be the brine with the least [Mg^{2+}] in halite, which did not precipitate much halite (high Na/Cl ratio) and where most Dead Sea brine compositions lie on its evaporation curve. The simulation ran based on the Pitzer database.

Input file:

```
TITLE Dead Sea evaporation
SOLUTION 1 Past Dead Sea
        units mol/kgw
        density 1.23
                                            temperature 30
        pH      6.0      # estimated
        Ca      0.16
        Mg      0.53
        Na      4.9
        K       0.1
        S(6)    0.005
        Cl      6.44
        Br      0.07
        C       1        CO2(g) -3.5

EQUILIBRIUM_PHASES

 # carbonates...

 CO2(g) -3.5 10; Calcite 0 0

 # sulfates...

 Gypsum 0 0;     Anhydrite 0 0;   Glauberite 0 0;
 Polyhalite 0 0

 Epsomite 0 0;   Kieserite 0 0;   Hexahydrite 0 0

 # chlorides...

 Halite 0 0;     Bischofite 0 0; Carnallite 0 0

REACTION

 H2O -1; 0 5*2 700*0.05

 INCREMENTAL_REACTIONS true

 SELECTED_OUTPUT 1

-file
                           DS_past_evap_FI.out
-water                                true
-totals                               Ca Mg Na K S(6)
Cl Br
-equilibrium_phases
 Halite Carnallite Gyspum Anhydrite
END
```

Appendix D. Uncertainties and other constraints on lake level and water discharge

The uncertainties in past climate reconstruction from the Dead Sea sediments and lake levels stem from the forcing factors that drive the lake-level changes, and how well it reflects changes in regional precipitation. Local precipitation over the lake surface is negligible compared to the runoff into the lake. The surface area of the lake (~700 km^2) is much smaller than its watershed (~40,000 km^2) and the lake itself is located in an arid climate. Since the evaporation from the lake is mainly controlled by salinity rather than temperature (e.g. Lensky et al., 2005), and the salinity did not change significantly during salt formation (Appendix C), the main factor controlling lake-level changes is the total water discharge into the lake.

Enzel et al. (2003) showed a high correlation between different rain stations in Israel and Dead Sea lake levels during the modern (instrumental) period. However, there is uncertainty involved in transitioning from "discharge into the lake" to "regional precipitation" in the past based on present-day climate and its sensitivity to temperature. Moreover, our model considers the bathymetry and topography of the Dead Sea basin and watershed to be similar to the present, and changes in these parameters add uncertainty to the lake-level reconstructions. Below we first detail the uncertainty in the lake-level reconstruction itself and then the uncertainty in interpreting precipitation from the lake level.

D.1. Uncertainties in lake-level reconstruction

Two important uncertainties are the depth of the basin over time (the subsidence rate) and the spatial distribution of halite.

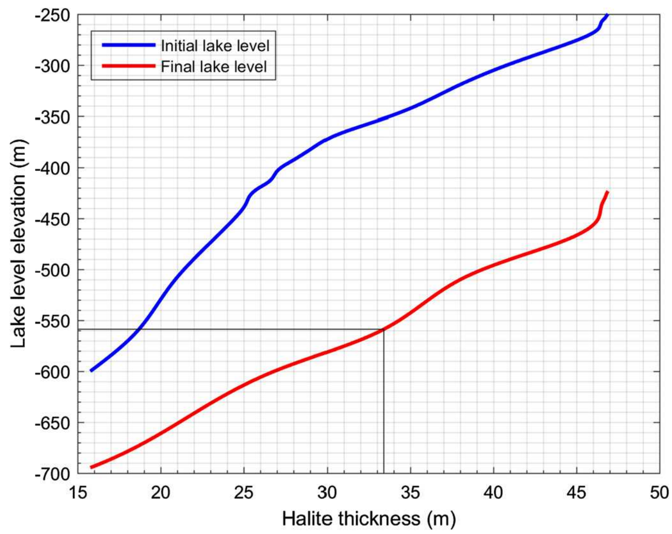

Fig. D1. Lake-level change as a function of halite thickness given the initial and final $[Mg^{2+}]$ and $[Na^{+}]$ during MIS 5e (Table 1) and a larger lake volume by $20 \cdot 10^9$ m^3.

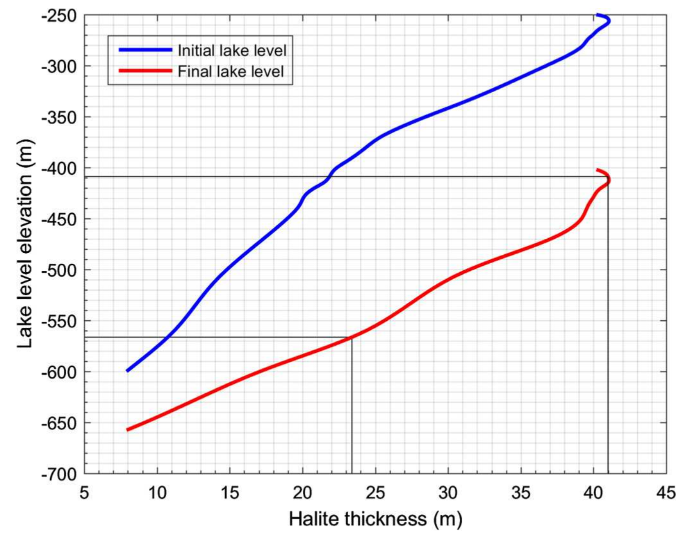

Fig. D2. Lake-level change as a function of halite thickness in MIS 5e, showing lake-level changes due to ±10 m of halite compared with the thicknesses in the DSDDP core.

In order to estimate the changes in the final lake level and thus the discharge into the lake, we calculated initial and final lake levels for different scenarios. In the case that the subsidence rate is lower than the sedimentation rate, the bottom of the lake during MIS 5e may have been deeper than today. Considering a lake bottom that is 200 m deeper than today (everything else being equal this requires $\sim 20^9$ m^3 of additional brine based on the hypsometric curve, Hall, 1997) with the MIS 5e parameters (Table 3), the resulting initial and final lake levels do not change significantly compared to the original scenario (the level would change from 350 to 560 mbsl vs. 320 to 490 mbsl; Fig. D1).

Other possible scenarios are associated with non-uniform halite deposition beneath the surface of the lake. For example, halite might be distributed over a wider area than the final surface area of the lake, or concentrated in the middle of the lake without covering the whole surface area. In our calculations we assumed that during MIS 5e all the marginal halite is re-dissolved and precipitated in the middle of the lake (the thickness of halite is multiplied by the final surface area of the lake). In some cases marginal halite may not be completely dissolved (an example would be the Holocene salt along the margins, Stein et al., 2010); this would mean we would underestimate the amount of halite, and the thickness of halite should be multiplied by a larger surface area in order to estimate the true amount of halite. In this case, halite will begin to precipitate at higher lake levels, and our model would predict higher final lake levels (Fig. D2). A halite thickness of 40 meters during MIS 5e instead of 33 m indicates a lake-level decrease to ~430 mbsl (Figs. 10, D2) and a discharge of ~780 million m^3/y (Fig. 11), which is still below 50% of the modern rate. Similarly, more focused halite in the lake center suggests we should have multiplied the halite thickness by a smaller surface area and thus the discharge would be lower and, the climate would be drier.

We also tested the sensitivity to changes in the Na^{+} concentration, using the final Na^{+} concentration in the halite fluid inclusions (1.71 $mol\,L^{-1}$) instead of the concentration in the pore water (1.09 $mol\,L^{-1}$). This resulted in a decrease to a lake level of 475 mbsl (Fig. D3) instead of 490 mbsl.

D.2. Uncertainties in estimations of precipitation

The main uncertainty in the precipitation estimation is related to the relationship between precipitation and water discharge (i.e., the runoff fraction) in cases of increasing temperatures or changes

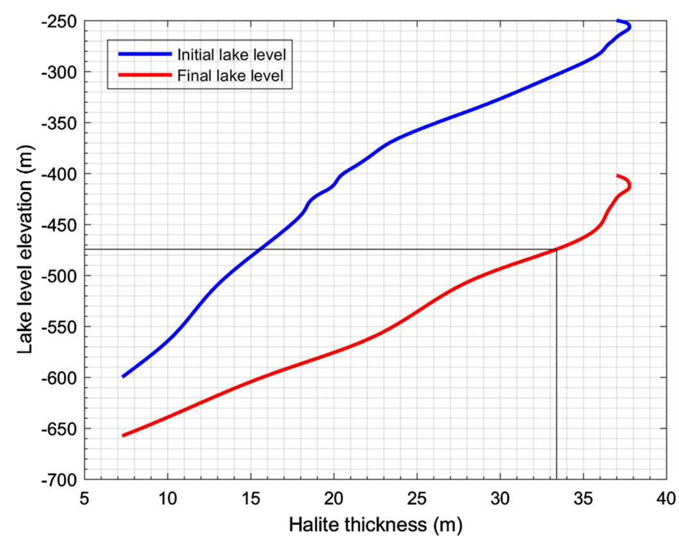

Fig. D3. Lake-level change with final Na^{+} concentration according to the halite fluid inclusion data (1.7 $mol\,L^{-1}$) during MIS 5e.

in the temporal and spatial variability of rainfall. The evapotranspiration in the watershed can increase by 10% due to increasing the temperature by 5°C (Scheff and Frierson, 2014) and thus average precipitation (in Jerusalem) interpreted from the discharge should be 10% higher than estimated and can reach 440 mm/y (73% of modern precipitation). Changes in the temporal distribution of both temperature and precipitation, including increased seasonality (e.g. Felis et al., 2004), may also affect the runoff fraction into the lake and thus the relationship between the discharge in the Jordan River and precipitation. The scatter in Fig. 11b covers at least part of this variability.

Precipitation can also vary spatially over relatively long time intervals, resulting in a different relationship between the discharge in the Jordan River and the total discharge to the Dead Sea, or a different relationship between the discharge in the Jordan River and rainfall in Jerusalem. Thus, our estimated rainfall amounts reflect the case that the spatial distribution was similar to the present.

Table D1
Constraints on fresh water sources and precipitation in the Dead Sea watershed as indicated from lake levels and halite intervals.

Lake level (m)	Jordan River discharge (10^6 m^3/y)	Precipitation in Jerusalem (mm/y)	Years/time (years)	Surface area (km^2)[a]	Discharge[b] (million m^3/y)	Evaporation rate (m/y)[c]	Remarks
−392[d]	1200[e]	550[f]	1931–1963	1000[e]	1600	1.6[g]	
−398[d]	960[h]	602[i]	1865–1885	940	∼1200–1500	1.3–1.6[g]	Meromictic structure and no halite precipitation
−402	<870[h]	<500		638	<1243	>1.3	Modern threshold for halite precipitation
−430[j]	500[h]	310	Holocene	590	710	1.2	

[a] Based on the hypsometric curve (Hall, 1997).
[b] Discharge is calculated from surface area and evaporation rate.
[c] Lensky et al. (2005), Stanhill (1994).
[d] Klein and Flohn (1987).
[e] Salameh and El-Naser (1999).
[f] Stable lake level according to Enzel et al. (2003).
[g] Evaporation rates of high lake stands are 1.3–1.6 m/y (Stanhill, 1994).
[h] Based on Jordan River discharge as 70% from total discharge (Salameh and El-Naser, 1999).
[i] Israel Metrological Service.
[j] Bookman (Ken-Tor) et al. (2004), Enzel et al. (2003), Migowski et al. (2006).

D.3. Independent constraints on water discharge

The modern Dead Sea dynamics provides constraints about water discharge. The modern threshold for halite precipitation is at ∼400 mbsl and a corresponding total discharge of ∼870 million m^3/y. Enzel et al. (2003) showed that a stable lake level corresponds to a precipitation rate of ∼550 mm/y in Jerusalem. During the time interval between 1931–1963, containing many observations and prior to major fresh source water diversions, the lake level was ∼395 mbsl, corresponding to a discharge of ∼1200 million m^3/y from the Jordan River, with a surface area of ∼1000 km^2 (Salameh and El-Naser, 1999).

Additional constraints on water discharge come from lake-level reconstructions. Comparison between lake levels and halite layers during the Holocene shows that in general halite precipitates when lake levels are low and are dropping (Fig. 12). Lake level decreased at least to 420-430 mbsl during several episodes during the Holocene (Bookman (Ken-Tor) et al., 2004; Migowski et al., 2006), corresponding to a water discharge of ∼700 million m^3/y (Table D1, Fig. 11). The amount of halite and the change in the chemistry (Eq. (5), Fig. 6) suggest that the major drop down to 450 mbsl occurred during the early Holocene before ∼6 ka (Fig. 12).

References

Ayora, C., Garcia-Veigas, J., Pueyo, J.-J., 1994. X-ray microanalysis of fluid inclusions and its application to the geochemical modeling of evaporite basins. Geochim. Cosmochim. Acta 58, 43–55. http://dx.doi.org/10.1016/0016-7037(94)90444-8.

Bar-Matthews, M., 2014. History of water in the Middle East and North Africa. In: Treatise on Geochemistry. Elsevier, pp. 109–128.

Bar-Matthews, M., Ayalon, A., Gilmour, M., Matthews, A., Hawkesworth, C.J., 2003. Sea–land oxygen isotopic relationships from planktonic foraminifera and speleothems in the Eastern Mediterranean region and their implication for paleorainfall during interglacial intervals. Geochim. Cosmochim. Acta 67, 3181–3199.

Bartov, Y., Goldstein, S.L., Stein, M., Enzel, Y., 2003. Catastrophic arid episodes in the Eastern Mediterranean linked with the North Atlantic Heinrich events. Geology 31, 439–442. http://dx.doi.org/10.1130/0091-7613(2003)031<0439:CAEITE>2.0.CO;2.

Bartov, Y., Stein, M., Enzel, Y., Agnon, A., Reches, Z., 2002. Lake levels and sequence stratigraphy of Lake Lisan, the Late Pleistocene Precursor of the Dead Sea. Quat. Res. 57, 9–21. http://dx.doi.org/10.1006/qres.2001.2284.

Battisti, D.S., Ding, Q., Roe, G.H., 2014. Coherent pan-Asian climatic and isotopic response to orbital forcing of tropical insolation. J. Geophys. Res., Atmos. 119, 11997–12020. http://dx.doi.org/10.1002/2014JD021960.Received.

Bentor, Y.K., 1961. Some geochemical aspects of the Dead Sea and the question of its age. Geochim. Cosmochim. Acta 25, 239–260.

Berger, A., Loutre, M.F., 1991. Insolation values for the climate of the last 10 million years. Quat. Sci. Rev. 10, 297–317. http://dx.doi.org/10.1016/0277-3791(91)90033-Q.

Bookman (Ken-Tor), R., Enzel, Y., Agnon, A., Stein, M., 2004. Late Holocene lake levels of the Dead Sea. Geol. Soc. Am. Bull. 116, 555–571. http://dx.doi.org/10.1130/B25286.1.

Brauer, A., Allen, J.R.M., Mingram, J., Dulski, P., Wulf, S., Huntley, B., 2007. Evidence for last interglacial chronology and environmental change from Southern Europe. Proc. Natl. Acad. Sci. USA 104, 450–455. http://dx.doi.org/10.1073/pnas.0603321104.

Cane, T., Rohling, E.J., Kemp, A.E.S., Cooke, S., Pearce, R.B., 2002. High-resolution stratigraphic framework for Mediterranean sapropel S5: defining temporal relationships between records of Eemian climate variability. Palaeogeogr. Palaeoclimatol. Palaeoecol. 183, 87–101. http://dx.doi.org/10.1016/S0031-0182(01)00461-8.

Cook, B.I., Anchukaitis, K.J., Touchan, R., Meko, D.M., Cook, E.R., 2016. Spatiotemporal drought variability in the Mediterranean over the last 900 years. J. Geophys. Res., Atmos. 121, 2060–2074. http://dx.doi.org/10.1002/2015JD023929.

Cullen, H.M., deMenocal, P.B., 2000. North Atlantic influence on Tigris–Euphrates streamflow. Int. J. Climatol. 20, 853–863.

Damnati, B., 2000. Holocene lake records in the Northern Hemisphere of Africa. J. Afr. Earth Sci. 31, 253–262. http://dx.doi.org/10.1016/S0899-5362(00)00089-0.

deMenocal, P., Ortiz, J., Guilderson, T., Adkins, J., Sarnthein, M., Baker, L., Yarusinsky, M., 2000. Abrupt onset and termination of the African Humid Period. Quat. Sci. Rev. 19, 347–361. http://dx.doi.org/10.1016/S0277-3791(99)00081-5.

Develle, A.-L., Gasse, F., Vidal, L., Williamson, D., Demory, F., Van Campo, E., Ghaleb, B., Thouveny, N., 2011. A 250 ka sedimentary record from a small karstic lake in the Northern Levant (Yammoûneh, Lebanon). Palaeogeogr. Palaeoclimatol. Palaeoecol. 305, 10–27. http://dx.doi.org/10.1016/j.palaeo.2011.02.008.

Dutton, A., Lambeck, K., 2012. Ice volume and sea level during the last interglacial. Science 80 (337), 216–219.

Enzel, Y., Bookman (Ken-Tor), R., Sharon, D., Gvirtzman, H., Dayab, U., Ziv, B., Stein, M., 2003. Late Holocene climates of the Near East deduced from Dead Sea level variations and modern regional winter rainfall. Quat. Res. 60, 263–273. http://dx.doi.org/10.1016/j.yqres.2003.07.011.

Feliks, Y., Ghil, M., Robertson, A.W., 2010. Oscillatory climate modes in the Eastern Mediterranean and their synchronization with the North Atlantic oscillation. J. Climate 23, 4060–4079. http://dx.doi.org/10.1175/2010JCLI3181.1.

Felis, T., Lohmann, G., Kuhnert, H., Lorenz, S.J., Scholz, D., Pätzold, J., Al-Rousan, S.A., Al-Moghrabi, S.M., 2004. Increased seasonality in Middle East temperatures during the last interglacial period. Nature 429, 164–168. http://dx.doi.org/10.1038/nature02546.

Felis, T., Pätzold, J., Loya, Y., Fine, M., Nawar, A.H., Wefer, G., 2000. A coral oxygen isotope record from the northern Red Sea documenting NAO, ENSO, and North Pacific teleconnections on Middle East climate variability since the year 1750. Paleoceanography 15, 679–694. http://dx.doi.org/10.1029/1999PA000477.

Felis, T., Rimbu, N., 2010. Mediterranean climate variability documented in oxygen isotope records from northern Red Sea corals — a review. Glob. Planet. Change 71, 232–241. http://dx.doi.org/10.1016/j.gloplacha.2009.10.006.

Frierson, D.M.W., Lu, J., Chen, G., 2007. Width of the Hadley cell in simple and comprehensive general circulation models. Geophys. Res. Lett. 34, 1–5. http://dx.doi.org/10.1029/2007GL031115.

Frumkin, A., 1996. Uplift rate relative to base-levels of a salt diapir (Dead Sea Basin Israel) as indicated by cave levels. Geol. Soc. (Lond.) Spec. Publ. 100, 41–47.

García-Veigas, J., Rosell, L., Zak, I., Playà, E., Ayora, C., Starinsky, A., 2009. Evidence of potash salt formation in the Pliocene Sedom Lagoon (Dead Sea Rift, Israel). Chem. Geol. 265, 499–511. http://dx.doi.org/10.1016/j.chemgeo.2009.05.013.

Garcıa-Veigas, J., 1993. Geoquımica de inclusiones fluidas en formaciones salinas, Microanálisis Cryo-SEM-EDS. Universitat de Barcelona.

Givati, A., Rosenfeld, D., 2013. The Arctic Oscillation, climate change and the effects on precipitation in Israel. Atmos. Res. 132–133, 114–124. http://dx.doi.org/10.1016/j.atmosres.2013.05.001.

Govin, A., Capron, E., Tzedakis, P.C., Verheyden, S., Ghaleb, B., Hillaire-Marcel, C., St-Onge, G., Stoner, J.S., Bassinot, F., Bazin, L., Blunier, T., Combourieu-Nebout, N., El Ouahabi, A., Genty, D., Gersonde, R., Jimenez-Amat, P., Landais, A., Martrat, B., Masson-Delmotte, V., Parrenin, F., Seidenkrantz, M.-S., Veres, D., Waelbroeck, C., Zahn, R., 2015. Sequence of events from the onset to the demise of the Last Interglacial: evaluating strengths and limitations of chronologies used in climatic archives. Quat. Sci. Rev. 129, 1–36. http://dx.doi.org/10.1016/j.quascirev.2015.09.018.

Haliva-Cohen, A., Stein, M., Goldstein, S.L., Sandler, A., Starinsky, A., 2012. Sources and transport routes of fine detritus material to the Late Quaternary Dead Sea basin. Quat. Sci. Rev. 50, 55–70. http://dx.doi.org/10.1016/j.quascirev.2012.06.014.

Hall, J.K., 1997. Topography and bathymetry of the Dead Sea depression. In: Niemi, T.M., Ben-Avraham, Z., Gat, J.R. (Eds.), The Dead Sea – the Lake and Its Settings. In: Oxford Monographs on Geology and Geophysics, vol. 36, pp. 11–21.

Harrison, S.P., Prentice, I.C., Guiot, J., 1993. Climatic controls on Holocene lake-level changes in Europe. Clim. Dyn. 8, 189–200. http://dx.doi.org/10.1007/BF00207965.

Hazan, N., Stein, M., Agnon, A., Marco, S., Nadel, D., Negendank, J.F.W., Schwab, M.J., Neev, D., 2005. The late Quaternary limnological history of Lake Kinneret (Sea of Galilee). Israel. Quat. Res. 63, 60–77. http://dx.doi.org/10.1016/j.yqres.2004.09.004.

Herold, M., Lohmann, G., 2009. Eemian tropical and subtropical African moisture transport: an isotope modelling study. Clim. Dyn. 33, 1075–1088. http://dx.doi.org/10.1007/s00382-008-0515-2.

Hurrell, J.W., Kushnir, Y., Visbeck, M., 2001. The North Atlantic oscillation. Science 80, 291.

Katz, A., Starinsky, A., 2008. Geochemical history of the Dead Sea. Aquat. Geochem. 15, 159–194. http://dx.doi.org/10.1007/s10498-008-9045-0.

Kelley, C., Ting, M., Seager, R., Kushnir, Y., 2012. Mediterranean precipitation climatology, seasonal cycle, and trend as simulated by CMIP5. Geophys. Res. Lett. 39, L21703. http://dx.doi.org/10.1029/2012GL053416.

Kiro, Y., Goldstein, S.L., Lazar, B., Stein, M., 2016. Environmental implications of salt facies in the Dead Sea. Geol. Soc. Am. Bull. 128, 824–841. http://dx.doi.org/10.1130/B31357.1.

Kitagawa, H., Stein, M., Goldstein, S.L., Nakamura, T., Lazar, B., DSDDP Scientific Party, 2016. Radiocarbon chronology of the DSDDP core at the deepest floor of the Dead Sea. Radiocarbon, 1–12. http://dx.doi.org/10.1017/RDC.2016.120.

Klein, C., Flohn, A., 1987. Contribution to the knowledge in the fluctuations of the Dead Sea level. Theor. Appl. Climatol. 38, 151–156.

Kolodny, Y., Stein, M., Machlus, M., 2005. Sea-rain-lake relation in the Last Glacial East Mediterranean revealed by $\delta^{18}O$–$\delta^{13}C$ in Lake Lisan aragonites. Geochim. Cosmochim. Acta 69, 4045–4060. http://dx.doi.org/10.1016/j.gca.2004.11.022.

Krumgalz, B.S., Hecht, A., Starinsky, A., Katz, A., 2000. Thermodynamic constraints on Dead Sea evaporation: can the Dead Sea dry up? Chem. Geol. 165, 1–11.

Krumgalz, B.S., Magdal, E., Starinsky, A., 2002. The evolution of a chloride sedimentary sequence-simulated evaporation of the Dead Sea. Isr. J. Earth-Sci. 51, 253–267. http://dx.doi.org/10.1560/EL8J-PVU9-EH88-M083.

Kukla, G.J., Bender, M.L., de Beaulieu, J.-L., Bond, G., Broecker, W.S., Cleveringa, P., Gavin, J.E., Herbert, T.D., Imbrie, J., Jouzel, J., Keigwin, L.D., Knudsen, K.-L., McManus, J.F., Merkt, J., Muhs, D.R., Müller, H., Poore, R.Z., Porter, S.C., Seret, G., Shackleton, N.J., Turner, C., Tzedakis, P.C., Winograd, I.J., 2002. Last interglacial climates. Quat. Res. 58, 2–13. http://dx.doi.org/10.1006/qres.2001.2316.

Kushnir, Y., Stein, M., 2010. North Atlantic influence on 19th–20th century rainfall in the Dead Sea watershed, teleconnections with the Sahel, and implication for Holocene climate fluctuations. Quat. Sci. Rev. 29, 3843–3860. http://dx.doi.org/10.1016/j.quascirev.2010.09.004.

Lazar, B., Stein, M., 2011. Freshwater on the route of hominids out of Africa revealed by U–Th in Red Sea corals. Geology 39, 1067–1070. http://dx.doi.org/10.1130/G32257.1.

Lelieveld, J., Hadjinicolaou, P., Kostopoulou, E., Chenoweth, J., El Maayar, M., Giannakopoulos, C., Hannides, C., Lange, M.a., Tanarhte, M., Tyrlis, E., Xoplaki, E., 2012. Climate change and impacts in the Eastern Mediterranean and the Middle East. Clim. Change 114, 667–687. http://dx.doi.org/10.1007/s10584-012-0418-4.

Lensky, N.G., Dvorkin, Y., Lyakhovsky, V., Gertman, I., Gavrieli, I., 2005. Water, salt, and energy balances of the Dead Sea. Water Resour. Res. 41, W12418. http://dx.doi.org/10.1029/2005WR004084.

Levy, E.J., Stein, M., Lazar, B., Yechieli, Y., Gavrieli, I., Sivan, O., 2017. Pore fluids in Dead Sea sediment core reveal linear response of lake chemistry to global climate changes. Geology, G38685.1. http://dx.doi.org/10.1130/G38685.1. In press.

Lisiecki, L.E., Raymo, M.E., 2005. A Pliocene–Pleistocene stack of 57 globally distributed benthic $\delta^{18}O$ records. Paleoceanography 20, 1–17. http://dx.doi.org/10.1029/2004PA001071.

Lowenstein, T.K., Dolginko, L.A.C., García-Veigas, J., 2016. Influence of magmatic-hydrothermal activity on brine evolution in closed basins: Searles Lake, California. Geol. Soc. Am. Bull. 128. http://dx.doi.org/10.1130/B31398.1.

Machlus, M., Enzel, Y., Goldstein, S.L., Marco, S., Stein, M., 2000. Reconstructing low levels of Lake Lisan by correlating fan-delta and lacustrine deposits. Quat. Int. 73–74, 137–144. http://dx.doi.org/10.1016/S1040-6182(00)00070-7.

Mariotti, A., Zeng, N., Yoon, J.-H., Artale, V., Navarra, A., Alpert, P., Li, L.Z.X., 2008. Mediterranean water cycle changes: transition to drier 21st century conditions in observations and CMIP3 simulations. Environ. Res. Lett. 3, 44001. http://dx.doi.org/10.1088/1748-9326/3/4/044001.

Matmon, A., Fink, D., Davis, M., Niedermann, S., Rood, D., Frumkin, A., 2014. Unraveling rift margin evolution and escarpment development ages along the Dead Sea fault using cosmogenic burial ages. Quat. Res. 82, 281–295. http://dx.doi.org/10.1016/j.yqres.2014.04.008.

Mayewski, a. Rohling E. E, P., Curt Stager, J., Karlén, W., Maasch, a, K., David Meeker, L., Meyerson, E.a., Gasse, F., van Kreveld, S., Holmgren, K., Lee-Thorp, J., Rosqvist, G., Rack, F., Staubwasser, M., Schneider, R.R., Steig, E.J., 2004. Holocene climate variability. Quat. Res. 62, 243–255. http://dx.doi.org/10.1016/j.yqres.2004.07.001.

McGarry, S., Bar-Matthews, M., Matthews, A., Vaks, A., Schilman, B., Ayalon, A., 2004. Constraints on hydrological and paleotemperature variations in the Eastern Mediterranean region in the last 140 ka given by the δD values of speleothem fluid inclusions. Quat. Sci. Rev. 23, 919–934. http://dx.doi.org/10.1016/j.quascirev.2003.06.020.

Migowski, C., Agnon, A., Bookman, R., Negendank, J.F., Stein, M., 2004. Recurrence pattern of Holocene earthquakes along the Dead Sea transform revealed by varve-counting and radiocarbon dating of lacustrine sediments. Earth Planet. Sci. Lett. 222, 301–314. http://dx.doi.org/10.1016/j.epsl.2004.02.015.

Migowski, C., Stein, M., Prasad, S., Negendank, J.F.W., Agnon, A., 2006. Holocene climate variability and cultural evolution in the Near East from the Dead Sea sedimentary record. Quat. Res. 66, 421–431. http://dx.doi.org/10.1016/j.yqres.2006.06.010.

Neev, D., Emery, K., 1995. The Destruction of Sodom, Gomorrah, and Jericho. Geological, Climatological, and Archaeological Background. Oxford University Press, New York.

Neugebauer, I., Brauer, A., Schwab, M.J., Waldmann, N.D., Enzel, Y., Kitagawa, H., Torfstein, A., Frank, U., Dulski, P., Agnon, A., Ariztegui, D., Ben-Avraham, Z., Goldstein, S.L., Stein, M., 2014. Lithology of the long sediment record recovered by the ICDP Dead Sea Deep Drilling Project (DSDDP). Quat. Sci. Rev. 102, 149–165. http://dx.doi.org/10.1016/j.quascirev.2014.08.013.

Neugebauer, I., Schwab, M.J., Waldmann, N.D., Tjallingii, R., Frank, U., Hadzhiivanova, E., Naumann, R., Taha, N., Agnon, A., Enzel, Y., Brauer, A., 2015. Hydroclimatic variability in the Levant during the early last glacial (∼117–75 ka) derived from micro-facies analyses of deep Dead Sea sediments. Clim. Past Discuss. 11, 3625–3663. http://dx.doi.org/10.5194/cpd-11-3625-2015.

Osborne, A.H., Vance, D., Rohling, E.J., Barton, N., Rogerson, M., Fello, N., 2008. A humid corridor across the Sahara for the migration of early modern humans out of Africa 120,000 years ago. Proc. Natl. Acad. Sci. USA 105, 16444–16447. http://dx.doi.org/10.1073/pnas.0804472105.

Otto-Bliesner, B.L., Rosenbloom, N., Stone, E.J., Mckay, N.P., Lunt, D.J., Brady, E.C., Overpeck, J.T., 2013. How warm was the last interglacial? New model–data comparisons. Philos. Trans. R. Soc., Math. Phys. Eng. Sci. 371, 1–20.

Paillard, D., Labeyrie, L., Yiou, P., 1996. Macintosh Program performs time-series analysis. Eos, Trans. Am. Geophys. Union 77, 379. http://dx.doi.org/10.1029/96EO00259.

Parkurst, D.L., Appelo, C.A.J., 2013. Description of input and examples for PHREEQC version 3—A computer program for speciation, batch-reaction, one-dimensional transport, and inverse geochemical calculations. In: U.S. Geological Survey Techniques and Methods, Book 6, p. 497.

Petit-Maire, N., Carbonel, P., Reyss, J.L., Sanlaville, P., Abed, A., Bourrouilh, R., Fontugne, M., Yasin, S., 2010. A vast Eemian palaeolake in Southern Jordan (29°N). Glob. Planet. Change 72, 368–373. http://dx.doi.org/10.1016/j.gloplacha.2010.01.012.

Pitzer, K.S., 1973. Thermodynamics of electrolytes. I. Theoretical basis and general equations. J. Phys. Chem. 77, 268–277. http://dx.doi.org/10.1021/j100621a026.

Prasad, S., Vos, H., Negendank, J.F.W., Waldmann, N., Goldstein, S.L., Stein, M., 2004. Evidence from Lake Lisan of solar influence on decadal- to centennial-scale climate variability during marine oxygen isotope stage 2. Geology 32, 581. http://dx.doi.org/10.1130/G20553.1.

Rohling, E.J., 2013. Quantitative assessment of glacial fluctuations in the level of Lake Lisan, Dead Sea rift. Quat. Sci. Rev. 70, 63–72. http://dx.doi.org/10.1016/j.quascirev.2013.03.013.

Rohling, E.J., Cane, T.R., Cooke, S., Sprovieri, M., Bouloubassi, I., Emeis, K.C., Schiebel, R., Kroon, D., Jorissen, F.J., Lorre, A., Kemp, A.E.S., 2002. African monsoon variability during the previous interglacial maximum. Earth Planet. Sci. Lett. 202, 61–75. http://dx.doi.org/10.1016/S0012-821X(02)00775-6.

Rosenberg, T.M., Preusser, F., Risberg, J., Plikk, A., Kadi, K.A., Matter, A., Fleitmann, D., 2013. Middle and Late Pleistocene humid periods recorded in palaeolake deposits of the Nafud desert, Saudi Arabia. Quat. Sci. Rev. 70, 109–123. http://dx.doi.org/10.1016/j.quascirev.2013.03.017.

Rossignol-Strick, M., 1985. Mediterranean Quaternary sapropels, an immediate response of the African monsoon to variation of insolation. Palaeogeogr. Palaeoclimatol. Palaeoecol. 49, 237–263. http://dx.doi.org/10.1016/0031-0182(85)90056-2.

Salameh, E., El-Naser, H., 1999. Does the actual drop in Dead Sea level reflect the development of water sources within its drainage basin? Acta Hydrochim. Hydrobiol. 27, 5–11.

Scheff, J., Frierson, D.M.W., 2014. Scaling potential evapotranspiration with greenhouse warming. J. Climate 27, 1539–1558. http://dx.doi.org/10.1175/JCLI-D-13-00233.1.

Seager, R., Liu, H., Henderson, N., Simpson, I., Kelley, C., Shaw, T., Kushnir, Y., Ting, M., 2014. Causes of increasing aridification of the Mediterranean Region in response to rising greenhouse gases. J. Climate 27, 4655–4676. http://dx.doi.org/10.1175/JCLI-D-13-00446.1.

Smith, J.R., Hawkins, A.L., Asmerom, Y., Polyak, V., Giegengack, R., 2007. New age constraints on the Middle Stone Age occupations of Kharga Oasis, Western Desert, Egypt. J. Hum. Evol. 52, 690–701. http://dx.doi.org/10.1016/j.jhevol.2007.01.004.

Stanhill, G., 1994. Changes in the rate of evaporation from the Dead Sea. Int. J. Climatol. 14, 465–471.

Starinsky, A., 1974. Interaction Between Calcium Chloride Brines and Sedimentary Rocks. The Hebrew University, Jerusalem.

Stein, M., 2001. The sedimentary and geochemical record of Neogene-Quaternary water bodies in the Dead Sea basin-inferences for the regional paleoclimatic history. J. Paleolimnol. 21, 271–282.

Stein, M., 2014. The evolution of Neogene-Quaternary water-bodies in the Dead Sea rift valley. In: Garfunkel, Z., Ben-Avraham, Z., Kagan, E. (Eds.), Dead Sea Transform Fault System: Reviews. Springer, pp. 279–316.

Stein, M., Ben-Avraham, Z., Goldstein, S.L., 2011. Dead Sea deep cores: a window into past climate and seismicity. Eos 92, 453–454. http://dx.doi.org/10.1111/j.2006.0906-7590.04596.x.Xiao.

Stein, M., Starinsky, A., Agnon, A., Katz, A., Raab, M., Spiro, B., Zak, I., 2000. The impact of brine-rock interaction during marine evaporite formation on the isotopic Sr record in the oceans: evidence from Mt. Sedom, Israel. Geochim. Cosmochim. Acta 64, 2039–2053. http://dx.doi.org/10.1016/S0016-7037(00)00370-7.

Stein, M., Starinsky, A., Katz, A., Goldstein, S.L., Machlus, M., Schram, A., 1997. Strontium isotopic, chemical, and sedimentological evidence for the evolution of Lake Lisan and the dead Sea. Geochim. Cosmochim. Acta 61, 3975–3992.

Stein, M., Torfstein, A., Gavrieli, I., Yechieli, Y., 2010. Abrupt aridities and salt deposition in the post-glacial Dead Sea and their North Atlantic connection. Quat. Sci. Rev. 29, 567–575. http://dx.doi.org/10.1016/j.quascirev.2009.10.015.

Szabo, B.J., Haynes, C.V., Maxwell, T.a., 1995. Ages of Quaternary pluvial episodes determined by uranium-series and radiocarbon dating of lacustrine deposits of Eastern Sahara. Palaeogeogr. Palaeoclimatol. Palaeoecol. 113, 227–242. http://dx.doi.org/10.1016/0031-0182(95)00052-N.

Torfstein, A., Gavrieli, I., Katz, A., Kolodny, Y., Stein, M., 2008. Gypsum as a monitor of the paleo-limnological-hydrological conditions in Lake Lisan and the Dead Sea. Geochim. Cosmochim. Acta 72, 2491–2509.

Torfstein, A., Gavrieli, I., Stein, M., 2005. The sources and evolution of sulfur in the hypersaline Lake Lisan (paleo-Dead Sea). Earth Planet. Sci. Lett. 236, 61–77. http://dx.doi.org/10.1016/j.epsl.2005.04.026.

Torfstein, A., Goldstein, S.L., Kagan, E.J., Stein, M., 2013. Integrated multi-site U–Th chronology of the last glacial Lake Lisan. Geochim. Cosmochim. Acta 104, 210–231.

Torfstein, A., Goldstein, S.L., Kushnir, Y., Enzel, Y., Haug, G., Stein, M., 2015. Dead Sea drawdown and monsoonal impacts in the Levant during the last interglacial. Earth Planet. Sci. Lett. 412, 235–244.

Torfstein, A., Haase-Schramm, A., Waldmann, N., Kolodny, Y., Stein, M., 2009. U-series and oxygen isotope chronology of the mid-Pleistocene Lake Amora (Dead Sea basin). Geochim. Cosmochim. Acta 73, 2603–2630. http://dx.doi.org/10.1016/j.gca.2009.02.010.

Vaks, A., Bar-Matthews, M., Ayalon, A., Matthews, A., Frumkin, A., Dayan, U., Halicz, L., Almogi-Labin, A., Schilman, B., 2006. Paleoclimate and location of the border between Mediterranean climate region and the Saharo-Arabian Desert as revealed by speleothems from the northern Negev Desert, Israel. Earth Planet. Sci. Lett. 249, 384–399. http://dx.doi.org/10.1016/j.epsl.2006.07.009.

Vaks, A., Bar-Matthews, M., Ayalon, A., Matthews, A., Halicz, L., Frumkin, A., 2007. Desert speleothems reveal climatic window for African exodus of early modern humans. Geology 35, 831–834. http://dx.doi.org/10.1130/G23794A.1.

Waldmann, N., Stein, M., Ariztegui, D., Starinsky, A., 2009. Stratigraphy, depositional environments and level reconstruction of the last interglacial Lake Samra in the Dead Sea basin. Quat. Res. 72, 1–15. http://dx.doi.org/10.1016/j.yqres.2009.03.005.

Waldmann, N., Torfstein, A., Stein, M., 2010. Northward intrusions of low- and mid-latitude storms across the Saharo-Arabian belt during past interglacials. Geology 38, 567–570. http://dx.doi.org/10.1130/G30654.1.

Wallace, J.M., 2000. North Atlantic oscillatiodannular mode: two paradigms – one phenomenon. Q. J. R. Meteorol. Soc. 126, 791–805. http://dx.doi.org/10.1002/qj.49712656402.

Wang, P., Tian, J., Lourens, L.J., 2010. Obscuring of long eccentricity cyclicity in Pleistocene oceanic carbon isotope records. Earth Planet. Sci. Lett. 290, 319–330. http://dx.doi.org/10.1016/j.epsl.2009.12.028.

Weinberger, R., Bar-Matthews, M., Levi, T., Begin, Z.B., 2007. Late-Pleistocene rise of the Sedom diapir on the backdrop of water-level fluctuations of Lake Lisan, Dead Sea basin. Quat. Int. 175, 53–61. http://dx.doi.org/10.1016/j.quaint.2007.03.007.

Yechieli, Y., Gavrieli, I., Berkowitz, B., Ronen, D., 1998. Will the Dead Sea die? Geology 26, 755–758.

Yechieli, Y., Magaritz, M., Levy, Y., Weber, U., Kafri, U., Woelfli, W., Bonani, G., 1993. Late quaternary geological history of the Dead Sea area, Israel. Quat. Res. 39, 59–67. http://dx.doi.org/10.1006/qres.1993.1007.

Yehudai, M., Lazar, B., Bar, N., Kiro, Y., Agnon, A., Shaked, Y., Stein, M., 2017. U–Th dating of calcite corals from the Gulf of Aqaba. Geochim. Cosmochim. Acta 198, 285–298.

Zak, I., 1967. The Geology of Mount Sedom. The Hebrew University, Jerusalem.

Zilberman-Kron, T., 2008. The Origin and Geochemical Evolution of Brines in the Sinkholes Along the Dead Sea Coast. The Hebrew University.